The Numb/p53 circuitry couples replicative self-renewal and tumor suppression in mammary epithelial cells

Daniela Tosoni,[1] Silvia Zecchini,[1] Marco Coazzoli,[1] Ivan Colaluca,[1] Giovanni Mazzarol,[1] Alicia Rubio,[1] Michele Caccia,[1] Emanuele Villa,[1] Olav Zilian,[2] Pier Paolo Di Fiore,[1,3,4]* and Salvatore Pece[1,4]*

[1]Istituto Europeo di Oncologia, 20141 Milan, Italy
[2]Helvea SA, 1207 Geneva, Switzerland
[3]Dipartimento di Scienze della Salute, Università degli Studi di Milano, 20142 Milan, Italy
[4]Fondazione Istituto FIRC di Oncologia Molecolare, 20139 Milan, Italy

The cell fate determinant Numb orchestrates tissue morphogenesis and patterning in developmental systems. In the human mammary gland, Numb is a tumor suppressor and regulates p53 levels. However, whether this function is linked to its role in fate determination remains unclear. Here, by exploiting an ex vivo system, we show that at mitosis of purified mammary stem cells (SCs), Numb ensures the asymmetric outcome of self-renewing divisions by partitioning into the progeny that retains the SC identity, where it sustains high p53 activity. Numb also controls progenitor maturation. At this level, Numb loss associates with the epithelial-to-mesenchymal transition and results in differentiation defects and reacquisition of stemness features. The mammary gland of Numb-knockout mice displays an expansion of the SC compartment, associated with morphological alterations and tumorigenicity in orthotopic transplants. This is because of low p53 levels and can be inhibited by restoration of Numb levels or p53 activity, which results in successful SC-targeted treatment.

Introduction

The structure of tissues is preserved by mechanisms that ensure the maintenance of the stem cell (SC) and progenitor cell compartments. These mechanisms are often altered in cancer (van de Wetering et al., 2002; Fre et al., 2005; Blanpain et al., 2006; Bouras et al., 2008; Karamboulas and Ailles, 2013). The homeostasis of several normal SC compartments rests on the ability of SCs to perform asymmetric self-renewing divisions in which one of the two daughter cells (DCs) retains the SC fate and withdraws into quiescence, whereas the other assumes a progenitor fate characterized by mitotic expansion and subsequent terminal differentiation (Lechler and Fuchs, 2005; Shinin et al., 2006; Bello et al., 2008; Bowman et al., 2008; Knoblich, 2010). This ensures the production of a large number of differentiated cells while limiting the size of the SC pool, and it likely represents a mechanism of tumor suppression. This latter notion is supported by evidence showing that skewing of the replicative mode from an asymmetric to a symmetric one (one SC → two SCs) is associated with tumorigenesis (Caussinus and Gonzalez, 2005; Cicalese et al., 2009).

Mechanisms underpinning asymmetric division rely on the unequal positioning of the two progeny relative to external cues (the "niche" concept) and/or on asymmetric partitioning of cell fate determinants during SC mitosis (Rhyu et al., 1994; Spana et al., 1995; Zhong et al., 1996; Lechler and Fuchs, 2005; Morrison and Kimble, 2006). In this second mechanism, a protein called Numb plays a critical role. By partitioning differentially between the two DCs, Numb controls their fate (Uemura et al., 1989; Rhyu et al., 1994; Zhong et al., 1996; Pece et al., 2011). The action of Numb has been attributed to its ability to antagonize the surface receptor Notch (Guo et al., 1996; Spana and Doe, 1996; McGill and McGlade, 2003; Pece et al., 2011). However, Numb is also able to stabilize p53 by interfering with its Mdm2-dependent ubiquitination and degradation (Colaluca et al., 2008). This might be relevant to SC homeostasis, because in isolated mammary stem cells, p53 imposes an asymmetric mode of self-renewal (Cicalese et al., 2009). Thus, the Numb-p53 axis might function as a tumor-suppressor pathway:

*P.P. Di Fiore and S. Pece contributed equally to this paper.

Correspondence to Pier Paolo Di Fiore: pierpaolo.difiore@ifom.eu; or Salvatore Pece: salvatore.pece@ieo.eu

Abbreviations used in this paper: Ab, antibody; CMV, cytomegalovirus; CSC, cancer stem cell; Ctr, control; DC, daughter cell; DsRed-Numb, Numb fused to the DsRed protein; EMT, epithelial-to-mesenchymal transition; FFPE, formalin-fixed paraffin-embedded; HAN, hyperplastic alveolar nodule; H&E, hematoxylin-eosin; IB, immunoblot; IF, immunofluorescence; IHC, immunohistochemistry; KD, knockdown; KO, knockout; MEC, mammary epithelial cell; MS, mammosphere; SC, stem cell; SCM, stem cell medium; SFE, sphere-forming efficiency; uGFP, unstable GFP protein; WT, wild type.

The Rockefeller University Press $30.00
J. Cell Biol. Vol. 211 No. 4 845–862
www.jcb.org/cgi/doi/10.1083/jcb.201505037

Numb asymmetric partitioning at mitosis could cause functional asymmetry of the Numb-p53 circuitry that would impart distinct developmental and proliferative fates to the two DCs.

Indeed, Numb expression is frequently attenuated in tumors (Pece et al., 2004; Colaluca et al., 2008; Westhoff et al., 2009). In breast cancers, one third of all tumors are Numb deficient, an event that correlates with aggressive disease and poor prognosis (Pece et al., 2004; Colaluca et al., 2008). Loss of Numb expression might well represent a major mechanism to override p53-mediated tumor suppression in these cancers, in which p53 mutations are relatively infrequent (Pharoah et al., 1999), by causing a reduction in p53 activity and skewing self-replicative divisions from an asymmetric to a symmetric mode. If so, the restoration of the Numb-p53 axis in Numb-deficient tumors should constitute an effective SC-targeted therapy. Finally, the predominant distribution of Numb in the luminal, as compared with the myoepithelial, layer of the normal mammary gland (Pece et al., 2004), argues that Numb might exert a role also in the control of progenitor maturation and terminal differentiation. The present study was undertaken to test these hypotheses.

Results

Numb partitions asymmetrically at the mitosis of PKH^{high} cells

By using the PKH (named for its discoverer, Paul Karl Horan) methodology combined with the mammosphere (MS) culture assay (Cicalese et al., 2009; Pece et al., 2010; Fig. S1, A–D), we have previously described the purification of a small population of cells (henceforth PKH^{high} cells) from the human or the murine mammary gland that display the characteristics expected of SCs. In these cells, Numb partitions unequally during mitosis (Cicalese et al., 2009; Pece et al., 2010; Fig. 1, A and B). To verify whether Numb segregates into the DC that retains SC-like properties or into the DC that displays progenitor-like behavior, mouse PKH^{high} cells from first-generation MS (see Fig. S1, E and F for a characterization of MS) were transduced with a lentiviral vector encoding Numb fused to the DsRed protein (DsRed-Numb) and monitored by time-lapse video microscopy. The mode of division was established by two criteria (Fig. 1 C and Materials and methods). (1) An initial asymmetric division of the PKH^{high} cell, followed by symmetric divisions of the progenitor, led to a typical 1–2-3-5 progression in the cell number; conversely, an initial symmetric division of the PKH^{high} cell led to a 1–2-4 pattern. (2) Retrospectively, the DC that retained SC-like characteristics was identified as the cell that remained quiescent and retained the PKH dye, whereas the progenitor divided further to yield a dull progeny; this pattern was clearly identifiable only when an initial asymmetric division had occurred, because a fully symmetric pattern of division led to progressive dilution of the dye. We found that PKH^{high} cells divided mainly asymmetrically and that Numb partitioned into the DC that retained SC-like characteristics (Fig. 1 D).

To guard against potential artifacts caused by excessive Numb-DsRed expression, we developed a more physiological setting based on the ablation of endogenous Numb followed by ectopic expression of Numb-DsRed under the control of a minimal cytomegalovirus (CMV) promoter (mCMV-Numb). To do this, cells dissociated from normal MS were transduced with an sh-oligo (sh-b; Fig. S2) to stably silence Numb and then transduced with mCMV-Numb or mock infected. This approach enabled reconstitution of Numb expression in Numb-knockdown (Numb-KD) cells to a level similar to the physiological one (Fig. S1 G). Also under these conditions, Numb partitioned asymmetrically in the stem-like DC at the first division of PKH^{high} cells (Fig. S1 H).

Numb expression in the mammary gland

To correlate these findings with the in vivo setting, we analyzed Numb distribution in the mouse mammary gland of 4-wk-old virgin females. This showed that, as observed in the normal human gland (Pece et al., 2004), Numb decorates the luminal epithelial layer of cytokeratin-8 (CK8)$^+$ cells, whereas it is excluded or expressed at low levels in the basal/myoepithelial layer of p63$^+$ cells (Fig. 2, A and B). Importantly, however, Numb was expressed in rare basal, p63$^+$ cells (Fig. 2, A and B) that, when occasionally dividing, showed asymmetric distribution of Numb to one of the progeny (Fig. 2, B–D). Conversely, in dividing luminal cells, Numb segregation was predominantly symmetric (Fig. 2, B–D).

These results show that in the mammary gland in vivo, there are at least two populations of Numb-expressing cells: one corresponding to bona fide luminal cells, in which Numb partitions symmetrically at mitosis, and the other, constituted by rare basal p63$^+$ cells present in the myoepithelial layer (which is in itself by and large Numb negative), in which Numb is asymmetrically segregated at mitosis similarly to what we observed in PKH^{high} cells.

To gain insight into the relationship between the two Numb-positive populations, we reverted to the ex vivo system and monitored Numb expression at different stages during MS formation. This revealed that, following the asymmetric partitioning of Numb at the mitosis of PKH^{high} cells, Numb is maintained at very low levels of expression in the early progeny (up to ∼4 d) and then progressively accumulates at later stages (Fig. 3, A–C), suggesting that, at least in vitro, Numb might exert a dual role in the PKH^{high} cell and in progenitors.

Numb controls asymmetric self-renewal in an ex vivo system

To investigate this possibility, we analyzed the consequences of Numb ablation. Because cytokeratin-5 (CK5) is a well-established basal layer marker (Shackleton et al., 2006; Stingl et al., 2006; Cicalese et al., 2009; Pece et al., 2010), we crossed Cre-loxP conditional Numb-knockout (Numb-KO) mice (Zilian et al., 2001; Wilson et al., 2007) with CK5-Cre mice (Ramirez et al., 2004). Primary mammary epithelial cells (MECs) established from these mice, and MS formed by them, displayed (a) markedly reduced Numb levels (Fig. 4 A), (b) decreased p53 levels and congruent alterations of positively (mdm2 and p21) and negatively regulated (nanog) p53 targets (Fig. 4, A and B), and (c) enhanced Notch activity measured by transcription of the Notch targets hey1 and hey2 (Fig. 4 B).

MS from wild-type (WT) MECs contained ∼300 cells/MS, with a sphere-forming efficiency (SFE) of ∼0.4% (Fig. 4 C). Thus, the frequency of MS forming units (MFUs) in WT-MS was ∼1:300, in agreement with previous reports (Cicalese et al., 2009). MS from Numb-KO MECs were approximately twofold larger (∼500 cells/MS) and showed an approximately twofold to threefold higher SFE, with an estimated frequency of ∼4–5 MFUs per MS (Fig. 4 C). Upon serial propagation, WT-MS progressively lost self-renewal ability

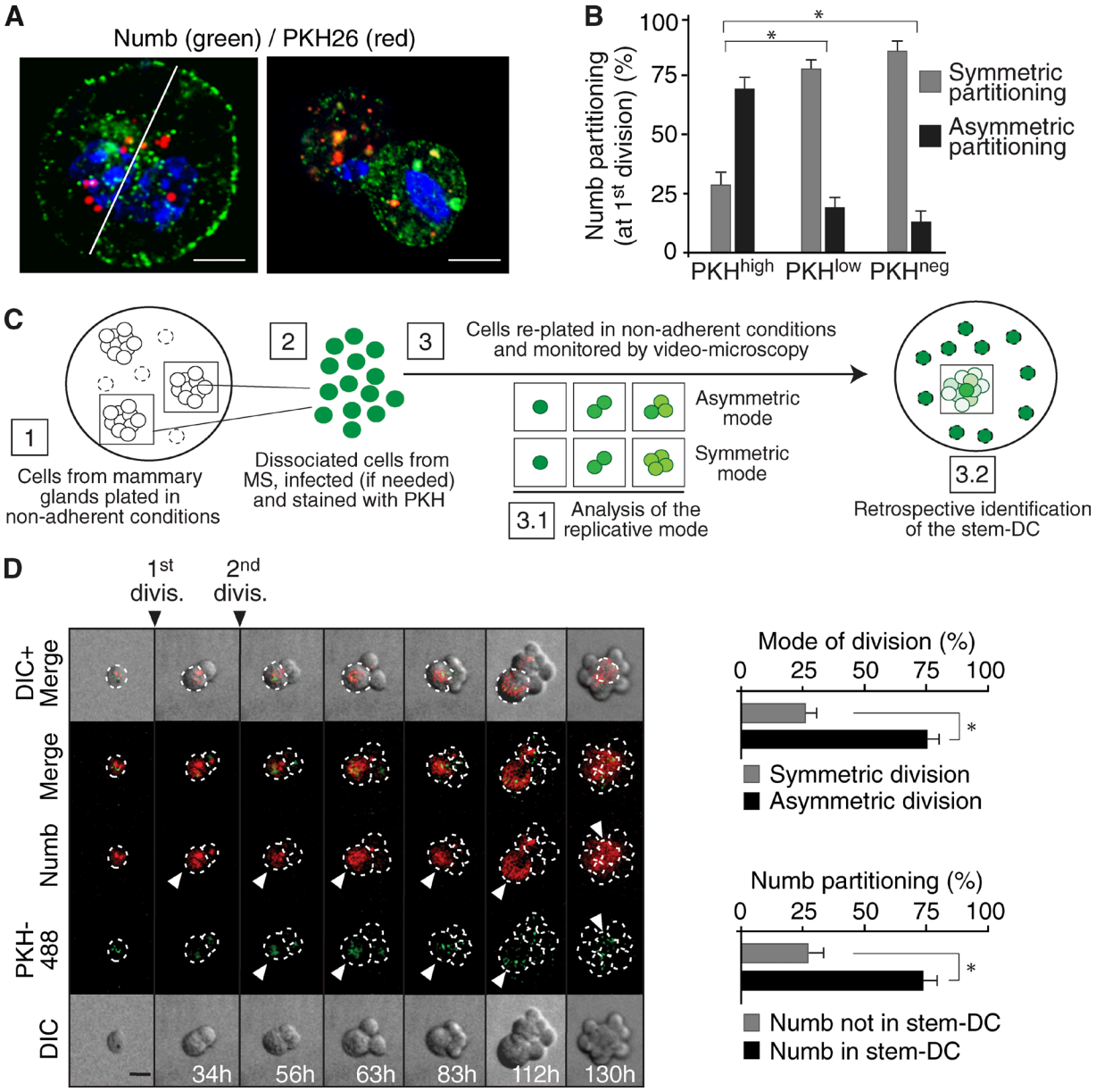

Figure 1. **Numb in the mitotic division of PKH^{high} cells.** (A) PKH^{high} cells (Fig. S1, A–D) were mock-treated (right) or treated with blebbistatin (left), which, by blocking cytokinesis (Straight et al., 2003), permits a better visualization of the endogenous Numb crescent at the plasma membrane, and stained with anti-Numb Ab and DAPI (blue). Bar, 5 µm. (B) Numb distribution in the three PKH fractions purified from MS (~100 cells analyzed per fraction). *, $P < 0.05$ versus the comparable condition (symmetric or asymmetric) in PKH^{high}. (C) Schematic of the methodology used to retrospectively assign cellular identity and mode of division; details are in Materials and methods. (D, left) Numb-DsRed–infected MS were dissociated, PKH-labeled (PKH488, green), and analyzed by video microscopy. Elapsed time is indicated. Arrowheads point to the stem-like DC. Bar, 10 µm. (right) Quantification of the divisional histories of PKH-labeled cells (top) and of the partition of Numb into the stem-like DC (bottom). The bar "Numb not in stem-DC" indicates Numb partitioned into the progenitor-DC or equally partitioned between the two daughters. *, $P < 0.05$.

(Fig. 4 D), consistent with previous reports (Cicalese et al., 2009; Pece et al., 2010). Conversely, the number of Numb-KO MS increased over time, with a constant approximately two-fold to threefold expansion rate (Fig. 4 D). Finally, during the formation of MS, Numb-KO cells divided predominantly in a symmetric fashion, and with a faster division rate compared with WT cells (Fig. 4 E). The entire set of observations was replicated using functional ablation (KD) of Numb in WT-MECs (Fig. S2). These observations argue that, at least in the ex vivo system herein used, Numb controls asymmetric self-renewal and lifespan of PKH^{high} cells, thus safeguarding against their uncontrolled expansion.

Numb controls p53 activity in PKH^{high} cells

We investigated the mechanisms through which Numb controls the fate of the progeny of PKH^{high} cells. We have previously shown that (a) the ratio of symmetric versus asymmetric divisions in PKH^{high} cells is controlled by p53 (Cicalese et al., 2009), and (b) Numb stabilizes the levels of p53 (Colaluca et al., 2008). Thus, because Numb partitions in the DC that retains stem-like features, it might function by positively modulating p53 activity in that cell. To investigate p53 activity, we used a p53 reporter containing multiple p53-binding sites upstream of a minimal CMV promoter to drive the expression of an unstable GFP protein (uGFP; half-life of ~60 min; Insinga et al.,

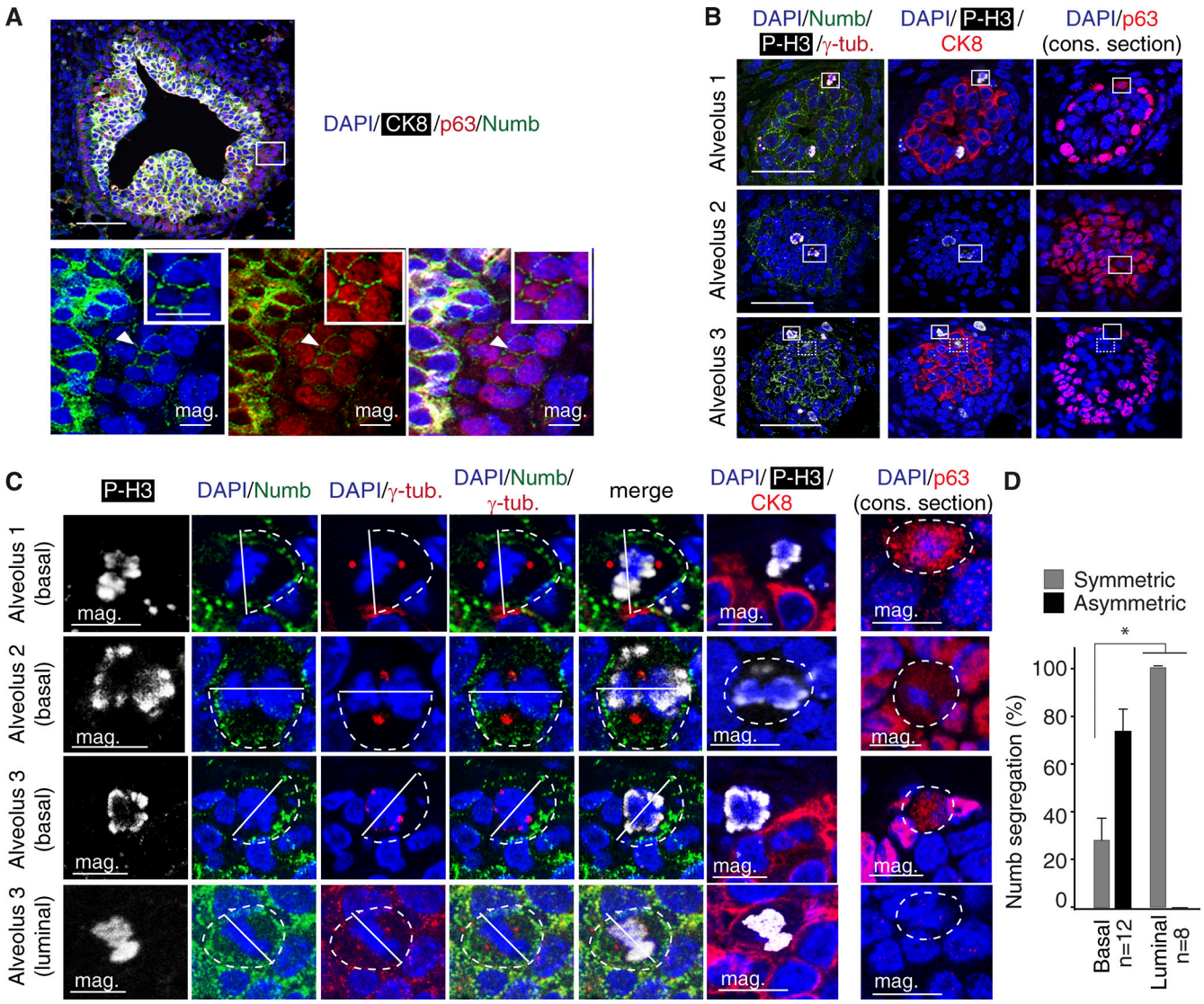

Figure 2. **Numb in the normal mouse mammary gland.** (A) Multichannel IF analysis of a murine mammary gland FFPE section using the indicated markers. The boxed area, in the top panel, is magnified in the bottom panels (mag.), with individual channels for each marker. The arrowhead points to a basal, p63+ cell expressing Numb (further magnified in the insets). CK8, white; p63, red; Numb, green; DAPI, blue. Bars: (top) 50 µm; (magnification and inset) 10 µm. (B) IF analysis of 4-wk-old mammary gland FFPE serial sections using the indicated markers (see Materials and methods for details). Three different alveoli are shown. The boxed areas indicate dividing cells (magnified below in C; four cells are boxed: three basal cells, boxed with a continuous line, and one luminal cell, boxed with a dashed line) in the luminal (CK8+) or in the basal (p63+) layer expressing the mitotic marker phosphorylated histone 3 (P-H3). P-H3, white; CK8, red; p63, red; Numb, green; DAPI, blue. The consecutive (cons.) section is indicated. Bar, 50 µm. (C) Magnifications of boxed areas in B. Top three rows (basal) show mitotic basal cells (see alveoli 1–3 in B) with asymmetric Numb crescent (dashed line). The cleavage plane (solid line) was deduced from the positions of the centrosomes. Note the diffuse cytoplasmic staining of p63 due to disassembly of the nuclear envelope. Bottom row (luminal) shows symmetric Numb crescents (dashed lines) during mitosis of a luminal, CK8+/p63− cell (see alveolus 3 in B). The consecutive (cons.) section is indicated. Bar, 10 µm. (D) Quantification of the experiment shown in B, displaying the frequency of Numb asymmetric/symmetric events in the indicated number of basal and luminal cells. *, $P < 0.05$ versus matched condition. Error bars are 95% confidence intervals.

2013). Cells from control (Ctr; mock silenced) or Numb-KD MSs were transduced with the p53-uGFP reporter, labeled with PKH, and allowed to reform MSs. Second-generation MSs were FACS purified, yielding a PKH^{high} (enriched in cells with SC-like characteristics) and a PKH^{neg} (enriched in progenitor-like cells) fraction (Cicalese et al., 2009; Pece et al., 2010). In Ctr populations, the p53-uGFP reporter activity was approximately twofold higher in PKH^{high} cells than in PKH^{neg} cells (Fig. 5 A, left), as also confirmed by direct detection of p53 protein levels (Fig. S3 A). Compared with Ctr-PKH^{high} cells, KD-PKH-^{high} cells showed approximately threefold lower overall levels of p53 activity (Fig. 5 A, right). Finally, we established that, during the initial phases of formation of a MS, p53 activity segregated with the PKH^{high} cell (Fig. 5 B) and cosegregated with Numb (Fig. 5 C). In Ctr-PKH^{high} cells, at the time of the first division, p53 activity was equally partitioned between the two DCs. Subsequently, however, the DC that retained stem-like properties reaccumulated high p53 activity levels, whereas the progenitor did not (Fig. 5 D). The accumulation of p53 activity was Numb dependent. Indeed, in Numb-KD PKH^{high} cells, there were overall lower levels of p53 activity and no evident signs of an increase in p53 activity in either DC (Fig. 5 E). These findings argue that the unequal partitioning of Numb at mitosis of PKH^{high} cells is reflected into a functional asymmetry of p53

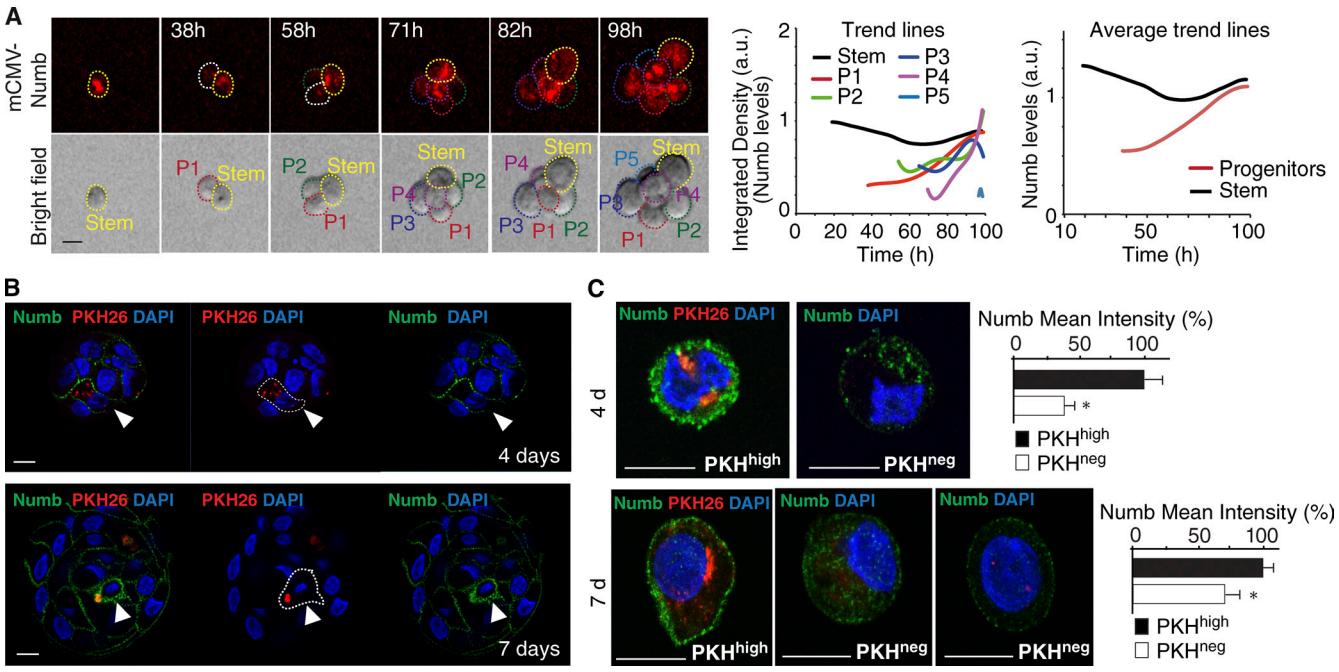

Figure 3. **Numb in progenitors.** (A) Numb-KD MS, reconstituted with mCMV-Numb, were dissociated and analyzed by video microscopy. (left) Frames of a typical tracking experiment are shown. Dashed lines identify the cellular identity (stem or P, progenitors, numbered 1–5 according to the order of appearance). Bar, 10 µm. (middle) Quantification of the experiment. Individual trend lines represent the integrated density calculated in each cell, as indicated. The trend line for P 5 is minimal, as this cell appeared at the end of the recording. (right) The mean trend lines represent the mean integrated Numb levels of all progenitors, shown in comparison to that of the stem cell (n = 3 videos from a single experiment). (B) The pattern of endogenous Numb distribution was analyzed in PKH-labeled WT MSs at different stages of formation by IF. Bar, 10 µm. Dotted lines, PKH^{high} cells. (C) Cells from 4- and 7-d MSs were FACS-sorted based on their PKH content and analyzed by IF. For Numb in PKH^{neg} cells from 7-d MSs (bottom panels), two representative images are shown to indicate that Numb expression in late progenitors is heterogeneous. Bar, 10 µm. Quantifications are shown in the rightmost panels. *, $P < 0.05$ versus PKH^{high}.

activity, likely required to control asymmetric self-renewal, at least under the ex vivo conditions herein used.

Restoration of p53 rescues the effects of Numb ablation

We used Nutlin3, an inhibitor of p53 ubiquitination/degradation (Vassilev et al., 2004), to test whether the restoration of p53 activity in Numb-KD cells could restore replicative asymmetry. Nutlin3 induced a dose-dependent increase of p53 expression in cells from dissociated Numb-KD MS (Fig. 6 A). This was accompanied by a reduction in the number and average size of Numb-KD MS, but not of Ctr MS (Fig. 6 B). Nutlin3 also impaired the ability of Numb-KD MS to expand in culture (Fig. 6 C) and caused a significant increase in asymmetric divisions (Fig. 6 D). The entire set of data obtained in Numb-KD cells was replicated in Numb-KO cells (selected experiments are in Fig. S3, B–D; a more detailed account is in Fig. 10). We could also demonstrate that (a) at the highest concentration used in our experiments (10 µM), Nutlin3 did not exert any apparent general antiproliferative or proapoptotic effect (Fig. S3 B), and (b) the effects of Nutlin3 were specific, as witnessed by experiments performed with an inactive enantiomer, Nutlin3b (Fig. S3, C and D).

Loss of Numb reprograms progenitors and differentiated cells to a SC-like state

Although the aforementioned findings define a role for Numb in PKH^{high} cells, the observations that Numb is increasingly expressed in proliferating progenitors (Fig. 3) and that it decorates the luminal layer in the adult gland (Fig. 2, A and B; Pece et al., 2004) argue for a role of Numb also at the level of progenitors and differentiated cells.

To analyze the consequences of Numb dysfunction at this level, we used a well-established protocol for immunophenotypical purification of various epithelial components from the mammary gland (Asselin-Labat et al., 2007; Guo et al., 2012). This protocol exploits the surface antigens CD49F and CD61 (Asselin-Labat et al., 2007; Guo et al., 2012) and allows the isolation of three populations: (1) basal cells ($CD49F^{high}/CD61^{+}$, enriched in SCs and also containing myoepithelial cells), (2) luminal progenitors ($CD49F^{low}/CD61^{+}$), and (3) differentiated luminal cells ($CD49F^{low}/CD61^{-}$; Fig. 7 A and Fig. S4 A). When the purification was performed in parallel in WT and KO glands, we observed, in the latter, increased frequency of SC-enriched basal cells and of immature luminal progenitors and a decrease in differentiated luminal cells (Fig. 7 B). This result suggests a role for Numb in maturation and luminal specification of progenitors. Thus, we used the CD49F/CD61 purification protocol and performed Numb silencing in the three populations to test them for self-renewal ability in MS serial propagation assays and for organotypic ability in 3D-Matrigel assays. 3D Matrigel outgrowths were also used as a source of cells for mammary fat pad reconstitution experiments in vivo. In SC-enriched basal cells, Numb ablation resulted in (a) increased MS-forming efficiency and self-renewal ability, compatible with a skewing from an asymmetric to a symmetric mode of division (Fig. 7 C); and (b) increased repopulation efficiency of the mammary fat pad in vivo (Fig. 7 D). In luminal progenitors and in terminally differentiated cells, Numb ablation resulted in the de novo acquisition of self-renewal potential in vitro (Fig. 7 C) and in vivo

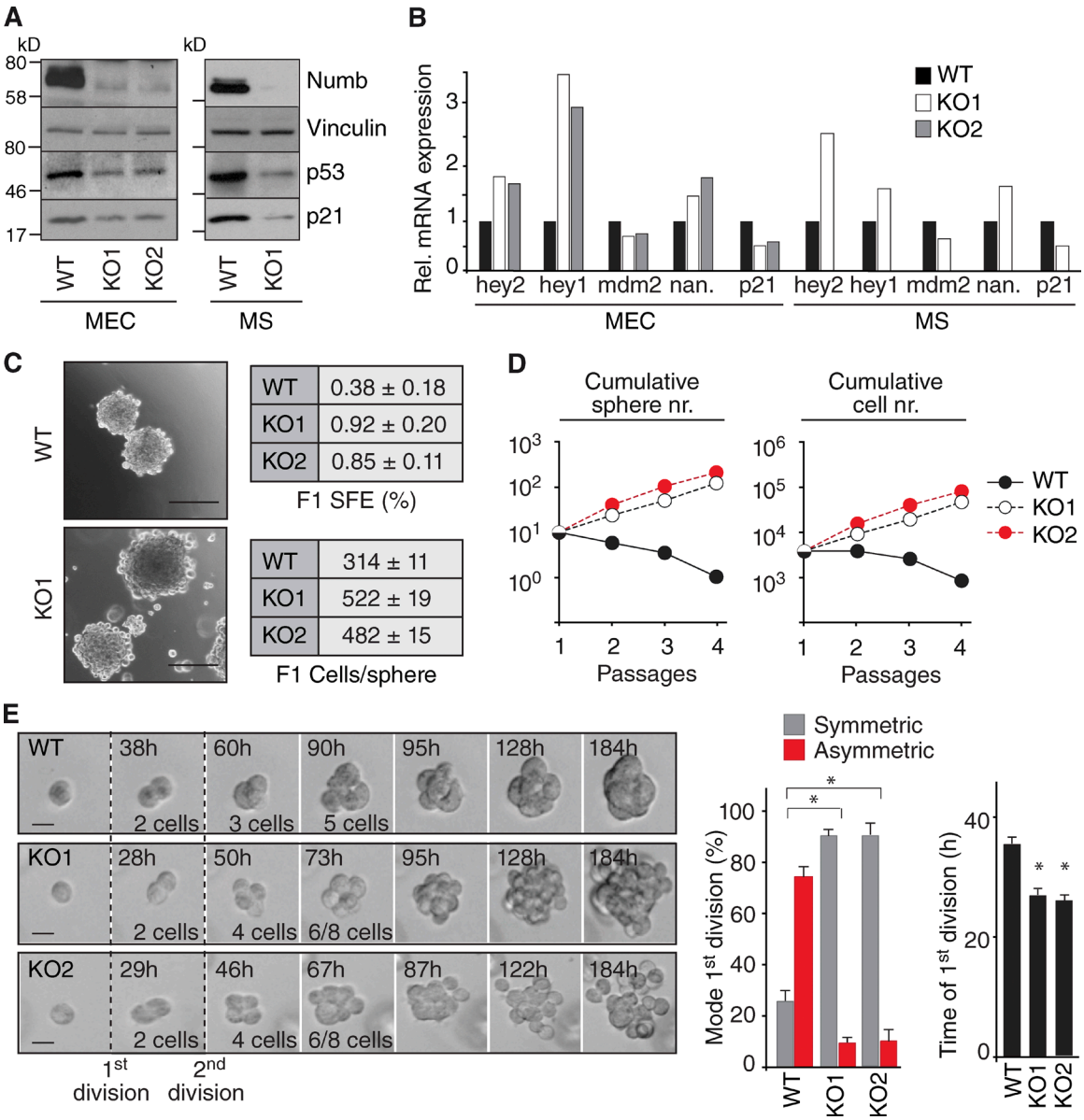

Figure 4. **Numb controls the replicative mode during MS formation.** (A) WT and Numb-KO (KO1 and KO2; see Fig. 9 for details) MECs or MS were analyzed by IB. (B) The indicated cells were analyzed by quantitative PCR. Data are from a single experiment run in triplicate and expressed relative to mRNA levels in WT cells (=1). Nan., nanog. (C, left) Representative images of WT and Numb-KO MS. Bar, 100 µm. Right, SFE and size (Cells/sphere) of WT and Numb-KO MS. (D) Cumulative sphere and cell number (nr.) from serial replating of WT and Numb-KO MS. A single representative experiment out of two repeats is shown. (E, left) Representative time-lapse video microscopy of the formation of WT or KO MS. Bar, 10 µm. (right) Quantification of the experiment. The mode and the time of the first division are shown. *, $P < 0.05$ versus comparable WT condition.

(Fig. 7 D). In all cases, transplantation of the Numb-KD populations yielded the formation of tumors, a finding that will be analyzed in depth later.

The organotypic 3D-Matrigel assays further revealed, in keeping with previous studies (Shackleton et al., 2006; Stingl et al., 2006), that (a) in MECs from the unperturbed mammary gland, basal cells with SC characteristics, present in the basal/myoepithelial fraction, generated filled-type structures; (b) progenitors formed hollow-type structures; and (c) differentiated luminal cells were devoid of organogenetic ability (Fig. 7, E and F; and Fig. S4 B). When KD populations were tested, we noticed (a) increased efficiency of formation of filled-type structures by basal MECs, (b) appearance of filled-type structures generated by KD progenitors, and (c) acquisition of de novo organogenetic ability by terminally differentiated cells, which formed both filled and hollow structures (Fig. 7, E and F; and Fig. S4 B). It is of note that the formation of disorganized, filled and hyperproliferative structures in 3D-Matrigel assays, besides being a typical phenotype of true SCs, is also associated with luminal progenitors that have undergone dedifferentiation and acquired stemness traits through the epithelial-to-mesenchymal transition (EMT; Mani et al., 2008; Guo et al., 2012). Consistent with this, we observed that depletion of Numb in the three FACS-sorted populations of SC-enriched basal cells, luminal progenitors, and luminal differentiated cells resulted in enhanced expression of EMT-associated transcription factors, evidenced both at the mRNA and protein levels (Fig. 7, G and H; and Fig. S4 C). Similar results were also obtained in

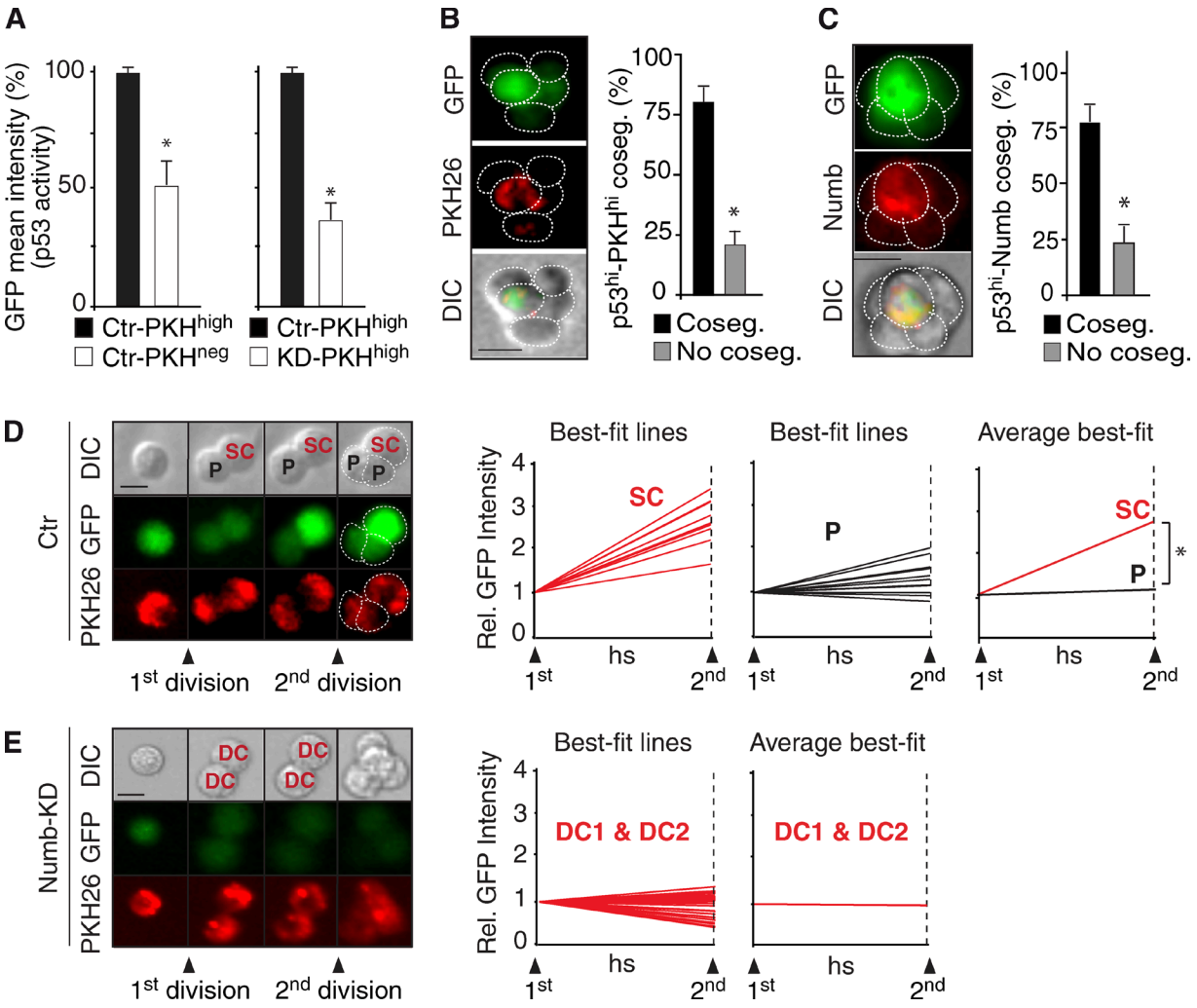

Figure 5. **Numb controls p53 activity.** (A) p53 activity in Ctr PKH^{high} and PKH^{neg} cells (left), and in PKH^{high} cells from Ctr or Numb-KD cells (right). Data are expressed as % of Ctr-PKH^{high} cells. *, P < 0.05 versus Ctr-PKH^{high} cells. (B and C) Cosegregation (Coseg.) of p53 activity (GFP) in PKH^{high} cells (B) and in Numb^{high} (Numb = Numb-DsRed) cells (C), during MS formation. Left panels, frames of a typical experiment. Right, quantifications; *, P < 0.05. (D) Fluorescence tracking of p53 activity (GFP) and PKH during the first and second divisions of WT (Ctr = mock-infected) PKH^{high} cells. (left) A typical example is shown. Bar, 10 µm. Right, quantifications. Individual best-fit lines represent the fluorescence intensity of SCs (n = 13) and progenitors (P, n = 13) between the first and second division. The "average best-fit" (rightmost) panel represents the mean of all SCs and P. *, P < 0.05. (E) Fluorescence tracking of p53 activity (GFP) and PKH during the first and second divisions of Numb-KD cells (n = 16, for a total of 32 tracks DC1 + DC2). Data are shown as in E. Because the two DCs of a Numb-KD PKH^{high} cell are indistinguishable, we referred to them as DC.

unfractionated Numb-KD MECs (Fig. S4 D). In this setting, a typical EMT transcriptional pattern could be reverted by ectopically expressed Numb-DsRed or by treatment with Nutlin3 (Fig. S4 D), pointing to the mechanistic implication of the Numb/p53 circuitry dysfunction in the occurrence of EMT.

These results argue that, at least under the ex vivo conditions of analysis herein used, Numb exerts a role at the progenitor compartment level, where Numb appears to suppress EMT and to ensure proper maturation and luminal cell fate specification. The results also demonstrate that loss of Numb reprograms, likely through EMT, progenitors and differentiated luminal cells to a SC-like state, eventually associated to tumorigenic potential.

Loss of Numb associates with aberrant mammary morphogenesis in vivo

These findings prompted us to evaluate the mammary gland of Numb-KO female mice. We initially analyzed the organogenetic ability of Numb-KO MECs, compared with WT, in 3D-Matrigel assays. The outgrowths generated by Numb-KO MECs displayed features of faulty morphogenesis, with disorganized, filled, and hyperproliferative structures, as opposed to the hollow-type acinar structures generated by WT MECs (Fig. 8, A and B). Consistent with this, histological analysis of 12-wk-old Numb-KO mammary glands invariably revealed, in comparison with WT glands, traits of aberrant morphogenesis, with gross morphological alterations consisting in ductal hyperplasia and ectasia, supernumerary lateral branching, and with the presence of areas of severe dysplasia, including hyperplastic alveolar nodules (HANs), which represent typical preneoplastic lesions (Medina, 1988; Skolnick et al., 1990; Jerry et al., 1993; Cardiff et al., 2000; Fig. 8, C–E). The Numb-KO mice, however, did not develop overt tumors, suggesting the need for additional events to develop the fully transformed phenotype (see Discussion). Numb-KO glands also displayed signs of aberrant lineage specification such as a marked increase in cells

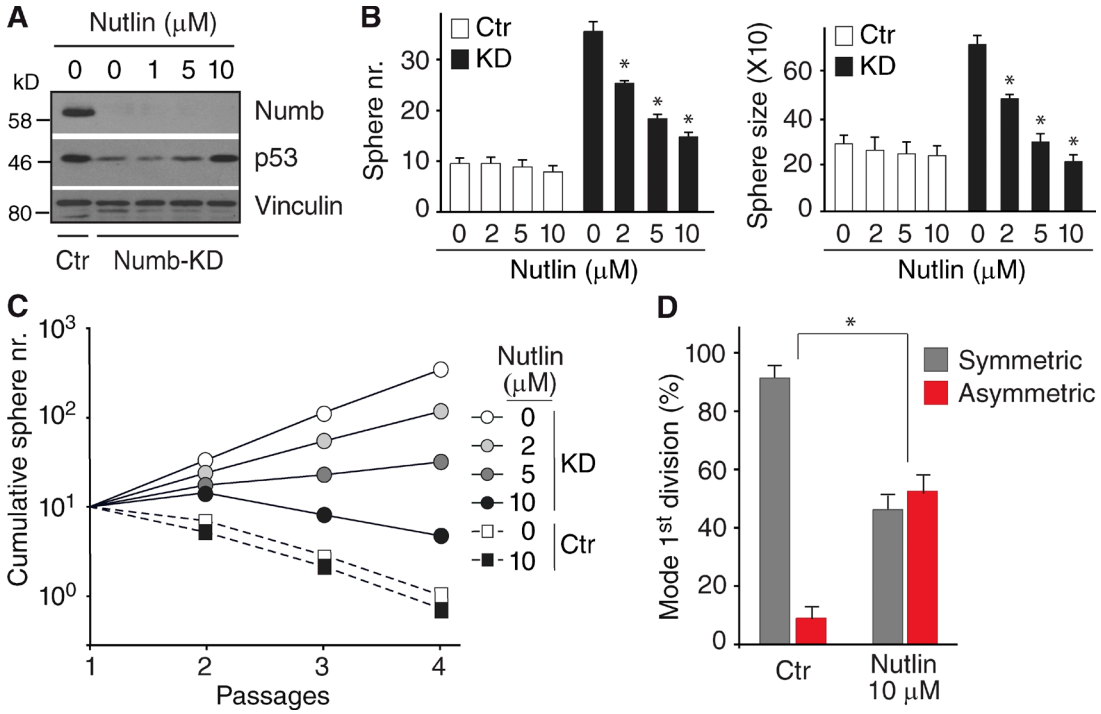

Figure 6. **Nutlin rescues the effect of Numb loss.** (A) Ctr and Numb-KD MS were treated with Nutlin3 followed by IB. (B) Sphere number (left) and size (right) of Ctr and Numb-KD MS in the presence of Nutlin3. *, $P < 0.05$ versus mock treatment. (C) Cumulative sphere number from serial replating of Ctr and Numb-KD MS in the presence of Nutlin3. A single representative experiment out of two repeats is shown. (D) Mode of the first division of Numb-KD MS-initiating cells in the absence (Ctr) or presence of 10 μM Nutlin3 (Nutlin) as obtained from time-lapse experiments. *, $P < 0.05$ versus matching mode of division in Ctr.

with concomitant expression of basal (CK14 or CD49F) and luminal (CK8) markers (Fig. 8 F and Fig. S4 E) and changes typically associated to EMT, such as decreased E-cadherin expression and increased frequency of cells positive for the transcription factors Sox9 and Slug (Fig. 8 G). We also noticed the appearance of $Slug^+$ cells outside the basal/myoepithelial layer, with the presence of cells showing concomitant Sox9 and Slug expression (Fig. 8 G), a trait associated with the de novo acquisition of a SC state via EMT-dependent dedifferentiation of progenitors (Guo et al., 2012).

Thus, Numb dysfunction results in profound alterations of the mammary morphogenetic program, with the emergence of signs of aberrant differentiation and the appearance of preneoplastic lesions.

Loss of Numb promotes tumorigenesis

Prompted by these results, we performed reconstitution experiments in cleared mammary fat pads using MECs, or dissociated MS, from Numb-KO and WT mice. We observed approximately fivefold more SCs in KO-derived populations than in WT (Fig. 9, A and B).

At the morphological level, the outgrowths generated by WT MECs and dissociated WT MSs were indistinguishable from the normal gland (Fig. 9 C, top), whereas those generated by Numb-KO cells displayed gross morphological alterations. We transplanted ten lines of MECs (or MS) from Numb-KO mice. In 7 of 10 cases, the reconstituted mammary tissue appeared hyperdense and hyperbranched (as exemplified by KO2; Fig. 9 C, middle) and displayed hyperplastic/dysplastic and preneoplastic lesions (HANs) and areas of frank malignancy (Fig. 9 D). In some cases (3 of 10), the outgrowths were overtly neoplastic (as exemplified by KO1; Fig. 9 C, bottom). The outcome of transplantation was an intrinsic property of each line, as individual MEC lines consistently gave rise either to an altered hyperplastic/dysplastic gland (always containing, however, malignant areas, e.g., KO2 in Fig. 9 C, middle) or to tumors (e.g., KO1 in Fig. 9 C, bottom). In all cases, the Numb-KO-driven expansion of the SC compartment was comparable, as witnessed by the similar efficiency of repopulation by KO1 and KO2 cells (Fig. 9, A and B; and see Fig. S5, A–C, for similar results obtained with Numb-KD cells). Histology of Numb-KO tumors invariably revealed signs of poor differentiation and high aggressiveness, such as loss of estrogen-receptor and E-cadherin and high expression of the proliferative marker PCNA (exemplified by KO1 in Fig. 9 E, left), accompanied by the presence of EMT traits (exemplified by KO1 in Fig. 9 E, right). The occurrence of EMT in these tumors was confirmed by the typical EMT transcriptional pattern displayed by Numb-KO MECs in vitro (Fig. 9 F). Of note, also in Numb-KO tumor cells, activation of the EMT program could be reverted by ectopically expressed Numb-DsRed (Fig. 9 F) or by treatment with Nutlin3 (Fig. 9 G).

Tumorigenesis by loss of Numb is p53 dependent

Impairment of p53 activity might be the mechanism responsible for the tumorigenic properties of Numb-KO MECs, a phenotype revertible, in principle, by Nutlin3. To test this, we selected the tumorigenic KO1 MEC line. Initially, we verified that the tumorigenicity of these cells was Numb dependent. Indeed, the ectopic expression of Numb-DsRed caused (a) restoration of p53 levels and function (Fig. 9 F), (b) decrease in SFE and MS size (Fig. 10 A), (c) reversion from symmetric to asymmetric

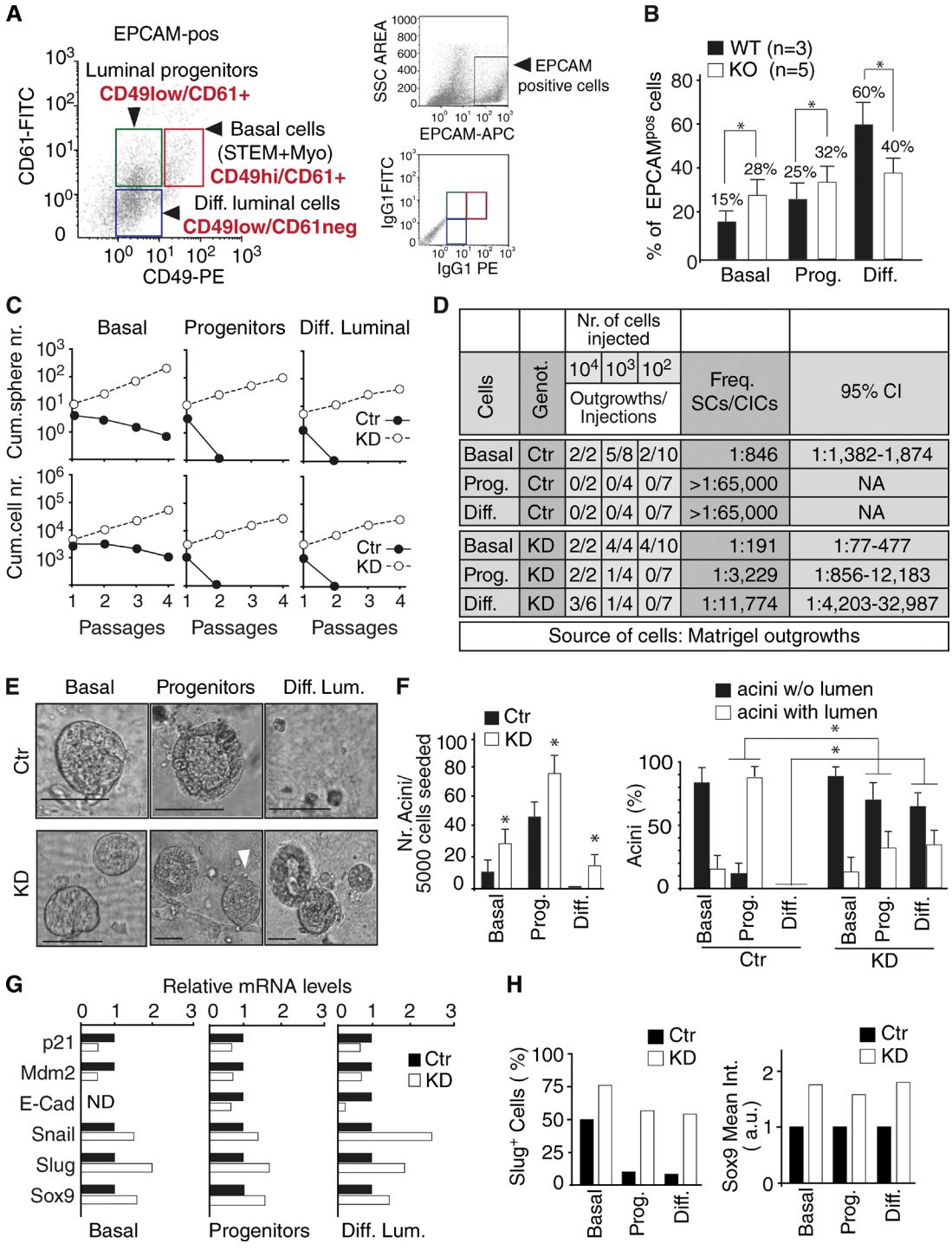

Figure 7. **Role of Numb in progenitors and differentiated cells.** (A, left) Representative FACS analysis performed on Lin⁻/EPCAM⁺ MECs using CD49F and CD61 to resolve the basal, immature progenitor, and luminal differentiated subsets. The boxes show the gating strategies used to obtain the fractions. (right) Gating strategy to discriminate EpCAM⁺ cells (top); (bottom) flow cytometry dot plot with boxes showing CD61⁺ and CD49F⁺ events back-gated on the EpCAM plot. (B) Proportion of the three fractions, isolated as in A, in WT versus Numb-KO glands. Data are the mean of the percentage of each fraction relative to the bulk population of EPCAM+ cells calculated independently in three WT and five Numb-KO mice. Error bars are 95% confidence intervals (see Materials and methods). *, $P < 0.05$ versus matching fraction in WT. (C) The three fractions were silenced for Numb (KD) or mock-silenced (Ctr) and subjected to an MS assay. A typical assay is shown reporting the cumulative sphere (top) and cell (bottom) number upon serial replating. (D) Mammary outgrowths, generated in 3D-Matrigel cultures from the different Ctr and KD MEC fractions were transplanted into NOD/SCID mice. The frequencies of SCs or cancer-initiating cells are shown, together with 95% confidence intervals. In all the cases, the Numb-KD MEC subfractions yielded tumors. (E) 3D-Matrigel outgrowths by Ctr or KD MEC fractions. In Ctr, basal cells formed typical filled structures (the organotypic ability in this fraction resides in the SC population), whereas progenitors formed hollow structures, and differentiated luminal cells displayed no organotypic ability but grew as bidimensional colonies or as small "filled" structures (diameter < 30 μm). In KD, luminal progenitors formed mainly filled-type structures (arrowhead in the middle panel), whereas differentiated luminal cells displayed de novo acquisition of organogenetic ability, with formation of both hollow and filled structures (Fig. S4 B). Bars, 100 μm. (F) Quantification of the experiment shown in E. Left, total number of outgrowths (acini) per 5,000 cells seeded. Data are the mean ± SD of

division (Fig. 9 B), and (d) reduction in tumorigenesis (Fig. 10 C). Cell proliferation or apoptosis of the bulk tumor population were not affected, suggesting a selective action of Numb on the intrinsic SC content (Fig. 10 D).

Next, cells dissociated from first-generation KO1 MSs were treated in vitro with Nutlin3. This caused (1) restoration of p53 levels and function (Fig. 9 G), (2) reduction in the number and size of MSs (Fig. 10 E), (3) increase in the frequency of SC asymmetric divisions (Fig. 10 F), and (4) reduction in tumorigenesis (Fig. 10 G). In a more stringent assay, we transplanted untreated KO1 cells and allowed tumors to reach a palpable size (~40 mm^3) before administering Nutlin3 in vivo. During this in vivo treatment, tumors in Nutlin3-treated mice continued to expand at the same rate as tumors in mock-treated mice (Fig. 10 H); however, upon retransplantation (in the absence of any further drug treatment), they displayed a decreased growth rate (~50%) with respect to tumors from mock-treated animals (Fig. 10 I), despite no evident effects on bulk tumor cell proliferation or apoptosis (Fig. 10 J). Of note, the SFE of tumor cells derived from Nutlin3-treated animals was similarly decreased compared with mock-treated animals (Fig. 10 K). Together, these results argue that restoration of the proficiency of the Numb/p53 circuitry yields a selective anticancer SC effect.

Discussion

Here, we demonstrate that Numb dysfunction contributes to mammary tumorigenesis by favoring the expansion of a pool of cells with stemness traits and intrinsic tumorigenic potential, operationally identifiable as cancer SCs. The biological and molecular bases of these phenotypes were dissected in an ex vivo setting in which cells displaying characteristics of SCs (PKH^{high} cells) divide asymmetrically, giving raise to progeny with different fates (Cicalese et al., 2009; Pece et al., 2010). Under these conditions, the ability of Numb to safeguard against the emergence of cancer stem cells (CSCs) is apparently caused by a dual level of action: in the PKH^{high} cell and in progenitors.

At the first mitosis of the PKH^{high} cell, Numb is partitioned into the DC that retains SC characteristics and imposes an asymmetric outcome to the self-renewing division, which prevents uncontrolled expansion. At present, we do not know whether Numb is asymmetrically partitioned in authentic SCs in vivo and whether this controls asymmetric divisional fate in the mammary gland. We have identified a population of $Numb^+$ cells in the basal layer in vivo, in which Numb is apparently asymmetrically segregated at mitosis. It remains to be established whether these cells are indeed SCs and, if so, whether the function of Numb in these cells is superimposable to the one that we characterized in the ex vivo setting.

In this latter setting, the action of Numb is mediated through regulation of the activity of p53. We showed that p53 activity is comparably segregated between the two DCs of a PKH^{high} cell but that it reaccumulates in the DC that retains stem-like features, though not in the progenitor. Because Numb inhibits p53 degradation (Colaluca et al., 2008), this argues that Numb stabilizes p53 in the stem-like DC. As a proof of this concept, we demonstrated that (a) in the absence of Numb, p53 activity is strongly decreased in the SC and in its progeny; (b) in the absence of Numb, the asymmetric reaccumulation of p53 activity in the stem-like DC does not occur; (c) the Numb KO phenocopies the p53 KO; and (d) the relevant phenotypes of Numb KO can be rescued by restoration of p53 activity.

The homeostatic function of the Numb-p53 axis might simply be the result of the growth-suppressive ability of p53, which could contribute to the stem-like DC withdrawal into quiescence: a hallmark of stemness. However, whereas Numb (this paper) and p53 (Cicalese et al., 2009) clearly impose an alternative differentiative and proliferative fate on the progeny of PKH^{high} cells, it is less clear how subversion of the Numb-p53 circuitry influences the identity of the two DCs. The interpretation of the results here is not straightforward, as the two DCs display mixed stem (self-renewal) and progenitor (sustained proliferation) properties as an integral part of a tumorigenic phenotype. In the normal setting, at least in vitro, the mitotic retention of Numb clearly distinguishes, by the end of the PKH^{high} cell self-renewing division, the stem-like DC from the progenitor-DC, although we did not establish whether the low Numb levels in the progenitor-DC are associated with a basal versus luminal identity. However, the progressive increase in Numb expression in transiently amplifying progenitors, as recapitulated in the early stages of MS formation in vitro, and the observation that Numb is a luminal layer marker in the adult gland, suggest an additional role for Numb, and of p53, in luminal progenitors and luminal differentiated cells. Here, in the ex vivo setting, Numb appears to be critical for immature progenitor differentiation, and its loss causes phenotypic plasticity and ectopic self-renewal ability at various stages of progenitor maturation, in association with the activation of the EMT.

We did not establish whether the molecular workings of Numb are different in the PKH^{high} cell and in progenitors. However, in our ex vivo analyses, ablation of Numb resulted in similar phenotypes when performed in a population of basal cells enriched in SCs or in progenitors, i.e., acquisition of cancer SC traits associated with the EMT, in a manner dependent on the downmodulation of p53. Thus, it is possible that the presence of Numb constitutes a tumor-suppressor barrier that acts, with similar molecular mechanisms, at two different cellular levels.

Consistent with this dual role established in vitro, the mammary glands of Numb-KO mice displayed amplification of the SC pool accompanied by EMT and failure to coordinate correctly mammary gland morphogenesis, as witnessed by the formation of dysmorphic and/or overtly neoplastic mammary tissue. We do not know whether dysfunction of the Numb/p53 axis is the sole mechanism responsible for all these phenotypes. We note that loss of Numb expression also causes unchecked Notch activity, an event relevant to the transformed phenotype of Numb-deficient human tumors (Pece et al., 2004; Colaluca et al., 2008; Westhoff

biological triplicates. *, P < 0.05 versus Ctr in each subpopulation. Right, type of acini formed. *, P < 0.05 versus Ctr in the matching (acini w/o or with lumen) condition. (G) The three MEC fractions, isolated as in A, were silenced for Numb (KD) or mock-silenced (Ctr) and analyzed by quantitative PCR. Data are from a single experiment run in triplicate and expressed relative to mRNA levels in Ctr cells (=1). E-Cad, E-cadherin (in basal cells, E-cadherin was not detectable [ND]). *, P < 0.05 versus Ctr. (H) MEC fractions, isolated as in A and silenced for Numb (KD) or mock-silenced (Ctr), were analyzed by IF for the expression of Sox9 and Slug (images are in Fig. S4 C). The percentage of $Slug^+$ cells (left) and the mean intensity, expressed as arbitrary units (a.u.), of Sox9 (right) in the MEC fractions is displayed (>100 cells counted in four independent fields from a single experiment).

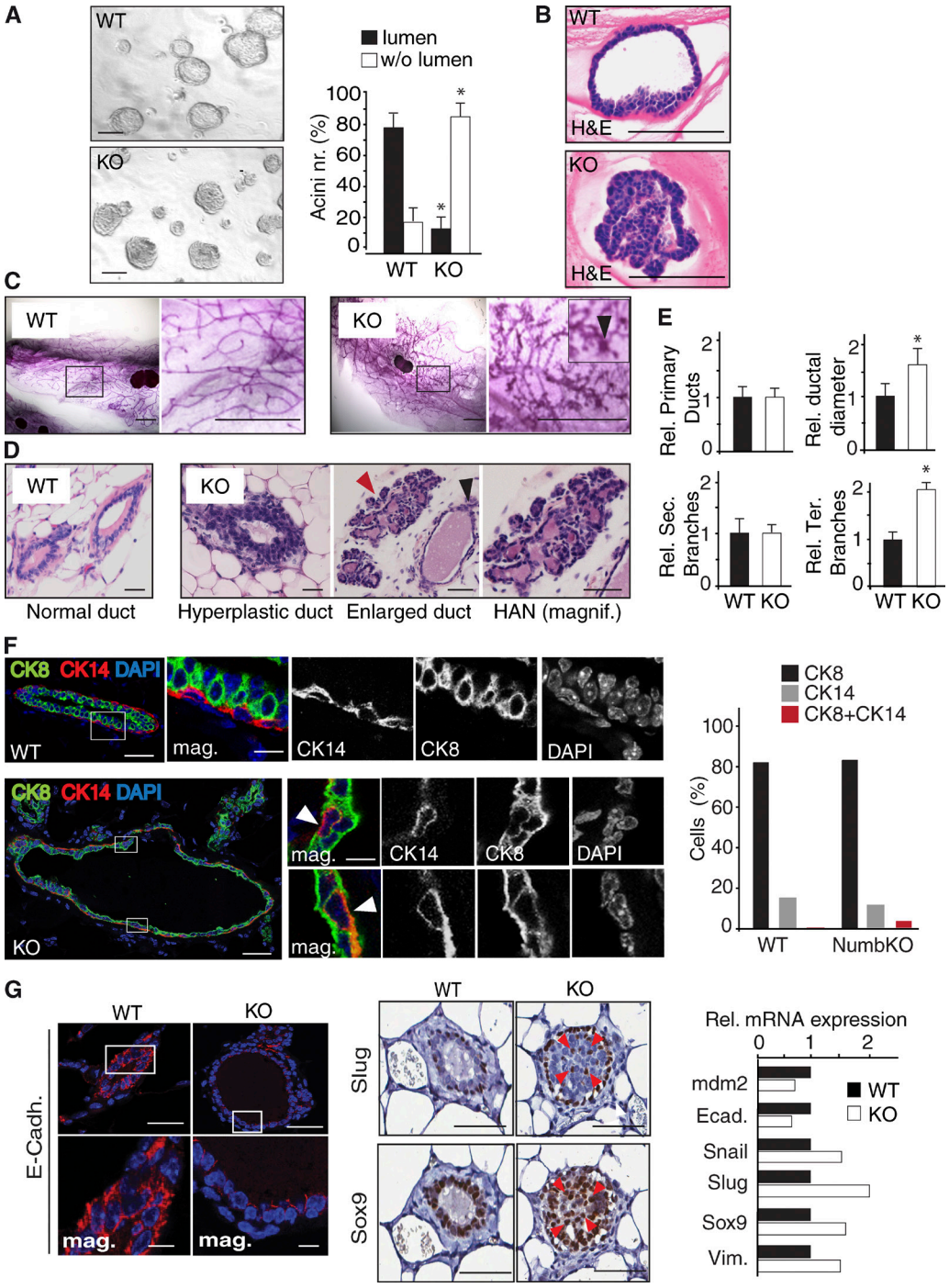

Figure 8. **Numb loss associates with aberrant morphogenesis and EMT in vivo.** (A) Morphology of colonies (acini), formed in 3D-Matrigel by WT and Numb-KO MECs. (left) Images of the 3D colonies in Matrigel. Bar, 100 µm. (right) Quantification of colonies with/without lumen. *, $P < 0.05$ versus WT. (B) Hematoxylin and eosin (H&E) staining of FFPE sections from 3D-Matrigel colonies showing the hollow-type versus the filled-type morphology of WT (top) and Numb-KO (bottom) outgrowths. Bar, 100 µm. (C) Carmine-stained whole-mounts of 12-wk-old mammary glands of virgin WT or Numb-KO mice. The boxed areas are magnified on the right. In the KO magnification panel, the arrowhead in the inset points to an area of HAN. Bar, 3.5 mm. (D) H&E staining of FFPE mammary glands of WT and Numb-KO mice. The black and red arrowheads point to an enlarged duct and an area of HAN, respectively. Bar, 50 µm. (E) Relative number of primary ducts, relative ductal diameter, and relative number of secondary and tertiary branches per mammary gland of Numb-KO and WT mice, expressed as % relative to WT. Data represent mean ± SD of three independent sets (five mice/each genotype). *, $P < 0.05$ versus WT. (F, left) Multichannel IF analysis of FFPE mammary glands of WT (top) or Numb-KO (bottom). Boxed areas are magnified on the right. In the Numb-KO glands, the arrowheads in the insets point to double CK14$^+$/CK8$^+$ cells. CK8, green; CK14, red; DAPI, blue. Bars: (main) 50 µm; (insets) 10 µm. (right) Percentage of single- and double-positive cells in WT and Numb-KO glands. Note the difference between double CK8$^+$/CK14$^+$ cells in WT (<1%) and Numb-KO glands (~5%). Data are from the analysis of >100 cells from a single experiment. (G) IF (left, E-cadherin) and IHC (middle, Slug, Sox9) analysis of FFPE sections from WT or Numb-KO glands. In the E-cadherin staining, the boxed areas are magnified at the bottom. Bars: (main) 50 µm; (insets) 10 µm. In the Slug/Sox9 images, the red arrowheads point to cells with concomitant Slug and Sox9 expression detected in 3-µm-thick serial FFPE sections of a Numb-KO gland. (right) WT and Numb-KO MECs were analyzed by quantitative PCR. Data are from a single experiment run in triplicate and expressed relative to mRNA levels in WT cells (=1). Vim., vimentin; Ecad., E-cadherin.

A

Source	Genot.	Nr. of cells injected: 10^5	10^4	$5x10^3$	10^3	10^2	10^1	Freq. SCs/CICs	95% CI
		Outgrowths/Injections							
MEC	WT	2/2	2/8	1/6	0/8	0/6	0/2	1:32,088	1:12,267-83,939
MEC	KO1	2/2	2/2	1/4	1/6	0/2	0/2	1:7,709	1:2,846-20,887
MEC	KO2	2/2	4/4	1/6	1/8	0/2	0/2	1:8,524	1:3,821-19,016

Source	Genot.	Nr. of cells injected: 10^5	10^4	10^3	$5x10^2$	10^2	10^1	Freq. SCs/CICs	95% CI
		Outgrowths/Injections							
MS	WT	2/2	2/2	2/2	4/8	3/10	0/6	1:492	1:245-987
MS	KO1	2/2	2/2	4/4	2/2	3/6	0/2	1:141	1:53-375
MS	KO2	2/2	4/4	4/4	5/6	4/8	0/2	1:207	1:101-428

B

Source	Genot.	Freq. SCs/CICs	Total Cells (glands/ mouse)	Fold-Increase in SCs (*vs.* WT)
MEC	WT	1: 32,088	980,000	1
MEC	KO1	1: 7,709	1,500,000	6,5
MEC	KO2	1: 8,524	1,630,000	6,4

Source	Genot.	Freq. SCs/CICs	Total Cells (mam.sph.)	Fold-Increase in SCs (*vs.* WT)
MS	WT	1: 492	314 ± 11	1
MS	KO1	1: 141	522 ± 19	5,8
MS	KO2	1: 207	482 ± 15	3,6

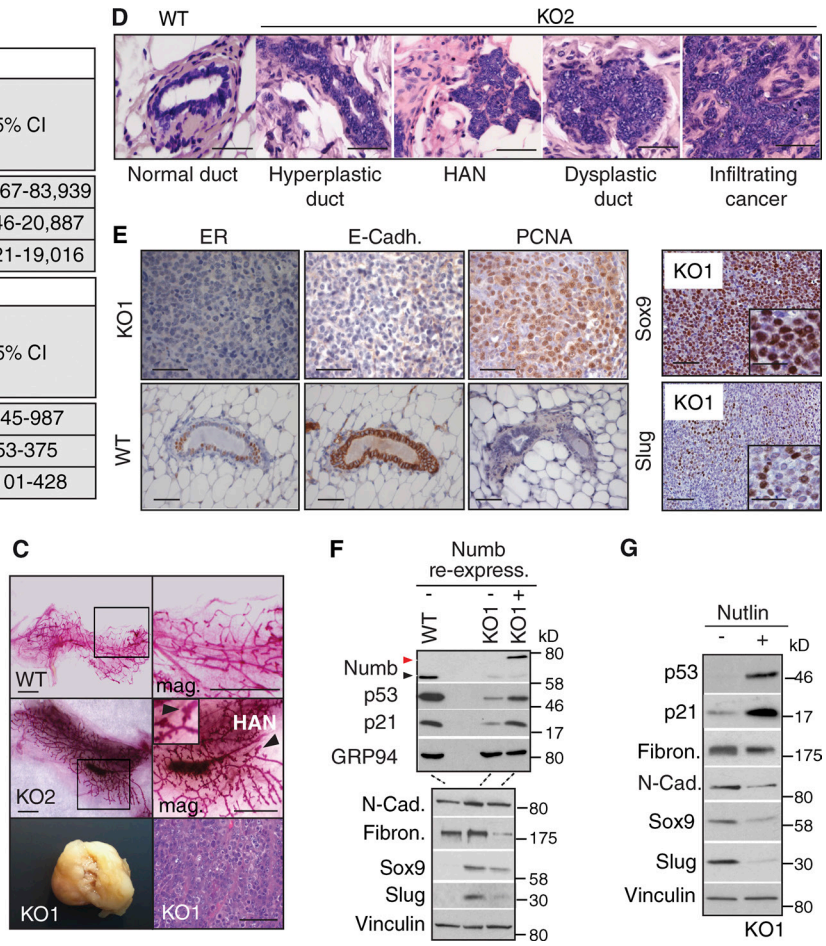

Figure 9. **Loss of Numb is tumorigenic.** (A) MECs or dissociated MSs (Source) derived from the indicated genotypes (Genot.) were orthotopically transplanted into immunocompromised mice. The frequencies of SCs or cancer-initiating cells are shown, together with 95% confidence intervals. KO1 is representative of the lines that gave rise to tumors; KO2 is representative of the lines that gave rise to aberrant mammary glands with areas of frank malignancy. (B, top) Data from A were recalculated after estimation of the total number of cells in the mammary gland/mouse, performed by digesting the pooled mammary tissues of individual mice and counting the cells. (bottom) The same calculations are reported for MS obtained from the indicated genotypes. (C, top and middle) Carmine-stained whole-mounts of outgrowths from WT or KO2 cells. The right panels show magnifications of the boxed areas (arrowheads and inset in KO2 images show an area of HAN). Bar, 3.5 mm. (bottom) A KO1-induced tumor is shown (left) with its histological appearance (right). Bar, 100 µm. (D) H&E staining of FFPE tissues from outgrowths generated by WT or KO2 MECs. Bar, 50 µm. (E) Left, IHC analysis of serial FFPE sections from a retransplanted KO1 tumor (top, KO1) or from a WT gland (bottom, WT). ER, estrogen receptor; E-Cadh., E-cadherin. Bar, 50 µm. Right, IHC analysis of serial FFPE sections from a retransplanted KO1 tumor. The magnified insets help visualizing Slug$^+$ and Sox9$^+$ cells. Bar, 50 µm. (F and G) Numb-KO1 cells were transduced with Numb-DsRed (KO1+Numb in F) or treated with 10 µM Nutlin3 (KO1+Nutlin in G), and compared with mock-infected (KO1 in F) or vehicle-treated (KO1 in G) cells, by IB. N-Cad, N-cadherin; Fibron., fibronectin. The red and black arrowheads (in F) indicate the overexpressed Numb-DsRed and the endogenous Numb proteins, respectively. The two IBs in F were loaded with the same lysates.

et al., 2009). Thus, deregulation of Notch activity might constitute an important factor, as also strongly suggested by evidence implicating Notch in the regulation of mammary SC self-renewal and in the proliferative/differentiative balance in progenitors (Weijzen et al., 2002; Raouf et al., 2008). In addition, our results indicate a gradient of alterations induced by Numb KO, from aberrant morphogenesis to preneoplastic lesions to various degrees of aggressiveness and tumorigenicity upon orthotopic transplantation. However, the Numb-KO mice did not develop frank tumors. This suggests the need for additional events to develop the fully transformed phenotype. The fact that epithelial cells from the KO gland were tumorigenic after reimplantation into the cleared fat pad of mice suggests that stromal components of the normal gland (or the architecture itself of the gland) might somehow suppress the development of a fully transformed phenotype.

In conclusion, our data argue that the Numb/p53 circuitry is a potent tumor-suppressor barrier against the appearance of CSCs. Therefore, Numb- or p53-targeted therapies should constitute SC-specific treatments in tumors displaying loss of Numb. This would be relevant to naturally occurring cancer, because in human breast cancers, one third of all tumors are Numb deficient (Pece et al., 2004; Colaluca et al., 2008). We demonstrated the proof of mechanism for such an approach by restoring p53 levels in vivo, with Nutlin3, in a Numb genetically null background. Under these conditions, the drug was ineffective on the growth of the primary tumor while being efficacious in dampening, in the absence of any further exposure to the drug, the growth of second-generation tumor transplants, a result compatible with what would be expected of a targeted anti-CSC therapy.

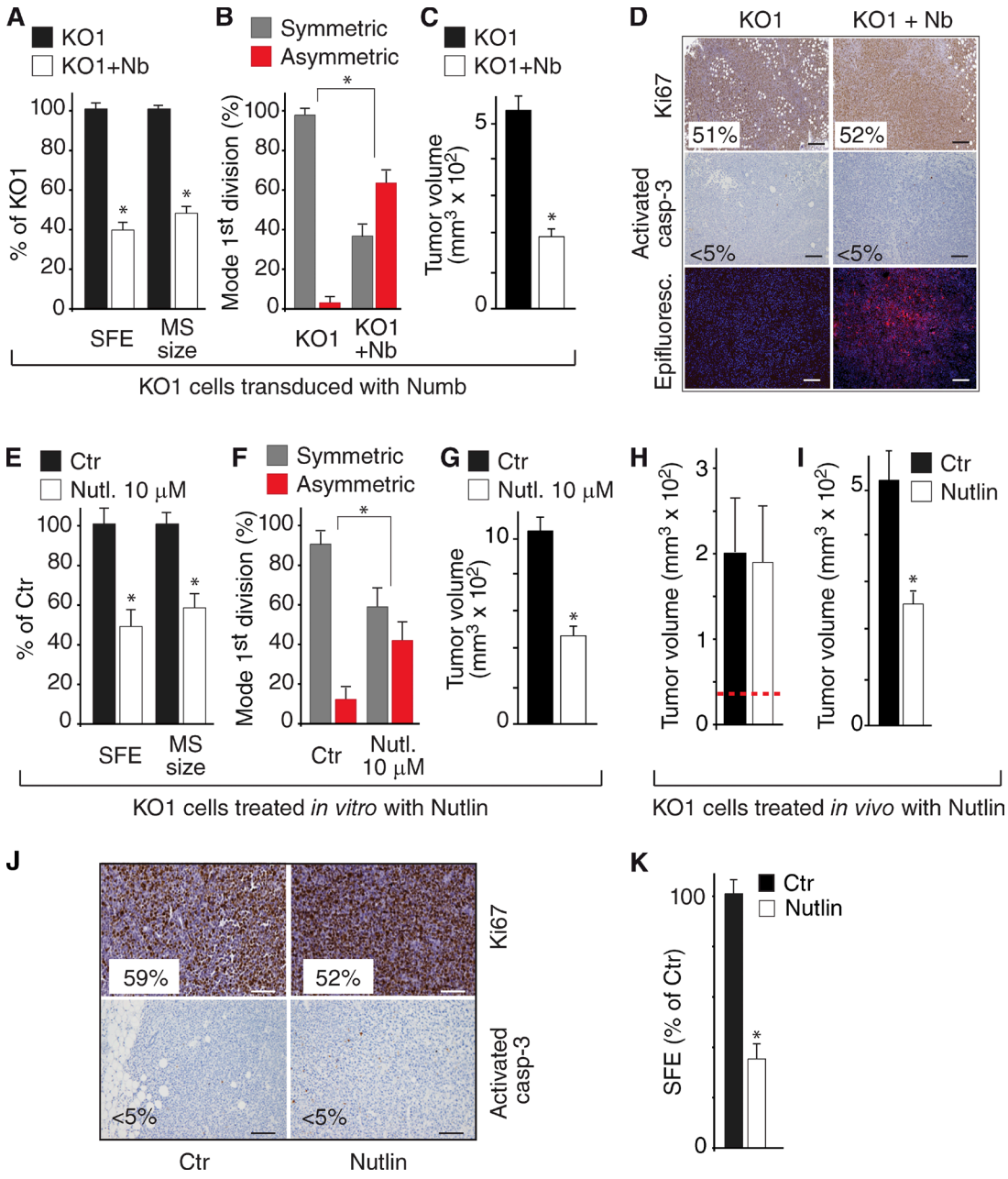

Figure 10. **Restoration of the Numb/p53 axis in Numb-deficient cells.** (A–D) SFE and MS size (A), mode of division (B), and tumorigenicity (C) of KO1 cells and KO1 cells transduced with Numb-DsRed (KO1+Nb). Protein levels for this experiment are shown in Fig. 9 F. *, $P < 0.05$ versus KO1 in the matching condition. Tumors from KO1 cells or from KO1 cells transduced with Numb-DsRed (KO1 + Nb) were analyzed by IHC as indicated (D); the percentage of positive cells is shown (>30,000 cells counted). The "Epifluorescence" panel shows the expression of Numb-DsRed in the KO1+Nb tumors. Bar, 100 µm. (E–G) SFE and MS size (E), mode of division (F), and tumorigenicity (G) of KO1 cells treated in vitro with 10 µM Nutlin3 or vehicle (Ctr). Protein levels for this experiment are shown in Fig. 9 G. *, $P < 0.05$ versus Ctr. (H) KO1 cells were orthotopically transplanted into immunocompromised mice and allowed to form tumors of ~40 mm^3 (dashed red line) before treatment with Nutlin3 or mock treatment (Ctr). At the end of the experiment, tumor size was measured. (I–K) Cells dissociated from tumors described in H were either retransplanted orthotopically in mice and left to grow for 3 wk (I) and analyzed by IHC (J) or tested for MS formation (K). *, $P < 0.05$ versus Ctr.

Materials and methods

Cell biology procedures and flow cytometry

Primary MECs were isolated from murine tissues and cultivated in suspension to yield first- (F1) or second-generation (F2) MSs, as described previously (Cicalese et al., 2009; Pece et al., 2010; Tosoni et al., 2012). In brief, murine mammary glands from FVB WT or Numb-KO mice were mechanically dissociated and digested in DMEM/F12 medium supplemented with 1 mM glutamine, 200 U/ml collagenase (Sigma-Aldrich), and 100 U/ml hyaluronidase (Sigma-Aldrich) at 37°C for 4 h. Cell suspensions were then centrifuged (80 *g*, 5 min), resuspended in 0.2% NaCl to lyse red blood cells, and sequentially filtered through membrane syringe filters of decreasing pore sizes (100-, 70-, 40-, and 20-µm meshes). Resulting cells were plated onto ultralow attachment plates (Falcon) at a density of 100,000 viable cells/ml (to obtain primary MS) in a stem cell medium (SCM) composed of serum-free mammary epithelial basal medium (Clonetics) supplemented with 5 µg/ml insulin, 0.5 µg/ml hydrocortisone, B27 (Invitrogen),

20 ng/ml EGF and bFGF (BD Biosciences), and 4 µg/ml heparin (Sigma-Aldrich). MS were collected after 6 d and mechanically dissociated by pipetting up and down several times with a fire-polished pipette to yield a single cell suspension. For serial MS propagation experiments, 5,000 cells derived from dissociation of primary MS were plated in quadruplicate in nonadherent conditions in SCM (liquid suspension culture) using 24-multiwell plates coated with a Poly HEMA (Sigma-Aldrich) solution (1.2% in 95% ethanol) or in SCM containing 1% methyl-cellulose. After 7 d, secondary MSs were counted and then dissociated to calculate the SFE (total number of MSs/total number of plated cells × 100). The same procedure was repeated to obtain subsequent MS generations over at least three more passages.

PKH labeling of MS was with PKH26 or PKH2-GL (PKH488) dyes (Sigma-Aldrich). Single-cell suspensions, from dissociated PKH-labeled MS, were FACS-sorted using a FACS Vantage SE flow cytometer (BD) equipped with a 488 nm laser (Enterprise Coherent) and a band-pass 575/26 nm optical filter (FL2 channel). A mean sorting rate of 1,000 events per second at a sorting pressure of 20 PSI was maintained.

For the purification of basal, progenitor, and terminally differentiated cells, single-cell suspensions, from mammary glands of 4- to 6-wk-old virgin mice, were lineage depleted with a cocktail of biotinylated antibodies (Abs) against CD5, CD45R, CD11b, GR-1 (Ly-6G/C), 7–4, and Ter-119 (Lineage Cell Depletion kit, #130-090-858; Miltenyi Biotec) and then FACS sorted using Abs against EpCAM (APC-conjugated 4G8.8 rat IgG2a; eBioscience), CD61 (FITC-conjugated hamster IgG1), and CD49F (PE-conjugated rat IgG2a) from BD Biosciences. Unstained cells were used as a negative control to establish the background fluorescence. To adjust the compensation, single stained Ctr cells were used for each dye used. Gating was initially applied to isolate single cell populations of viable cells, then additional gating was used to select for the bulk $EpCAM^+$ population. $EpCAM^+$ cells were then analyzed for the expression of CD61 and CD49F to resolve the different subsets of basal/myoepithelial ($EpCAM^+/CD49F^{high}/CD61^+$ cells), immature luminal progenitors ($EpCAM^+/CD49F^{low}/CD61^+$) and luminal differentiated ($EpCAM^+/CD49F^{low}/CD61^-$) cells. Flow cytometric analysis was performed using Kaluza Flow Analysis Software (Beckman Coulter). The purified MEC subfractions were infected with the silencing vector for Numb (see following paragraph) and used for MS propagation assays or for 3D-Matrigel organotypic cultures.

3D-Matrigel organotypic cultures were performed as previously described (Asselin-Labat et al., 2007; Guo et al., 2012), with minor modifications. In brief, single-cell suspensions from bulk MECs (~5,000 cells/well) or from FACS-purified MEC subfractions (~2,000 cells/well) were seeded in Poly-HEMA-coated four-well glass chamber slides (Chamber Slide System, 154526; Nunc) in a total volume of 700 µl mammary epithelial basal medium containing 5% Matrigel growth factor–reduced basement membrane matrix (354234; BD), supplemented with 2% heat-inactivated FBS, 10 ng/ml EGF, 20 ng/ml bFGF, 4 µg/ml heparin, and 2% B27. Cells were incubated at 37°C in the presence of 5% CO_2 for 14 d, with 300 µl fresh medium added every 7 d. The number of organotypic structures was counted 7–14 d after seeding. Resulting organotypic structures were observed and photographed using an inverted phase-contrast microscope equipped with a digital camera. To better visualize hollow- and filled-type structures, the organotypic outgrowths were fixed in 4% PFA for 1 h, stained with DAPI, and subjected to confocal analysis. When using 3D-Matrigel outgrowths for transplantation studies, the organotypic structures embedded in Matrigel were recovered by adding at each well of the chamber slide 1 ml ice-cold MatriSperse Cell Recovery Solution (354253; BD). After 1 h incubation on ice, the gel layers containing the structures were scraped and collected in a tube, rinsed with 1 ml BD Cell Recovery Solution, and incubated again for 30 min on ice and then centrifuged. The pellet containing the structures was washed with PBS and further digested with 0.05% trypsin for 10–15 min. The digested cells were then filtered through 40-µm cell strainers to obtain single cells. The cells were then counted, resuspended in ice-cold 1:1 PBS/phenol red-free growth-factor reduced Matrigel solution, and immediately transplanted into the mammary fat pad of immunocompromised mice.

Methodologies for the retrospective assignment of the cellular identity

The methodology used to retrospectively assign cellular identity and mode of division is illustrated in Fig. 1 C. Single-cell suspensions obtained from mammary glands were cultured in nonadherent conditions, as described above (Cicalese et al., 2009; Pece et al., 2010; Tosoni et al., 2012). Under these conditions, as shown in Fig. 1 C.1, most cells did not proliferate or underwent anoikis (represented by dashed circles), whereas SCs gave rise to MSs (represented by clusters of solid circles). MSs were then isolated and dissociated, infected with appropriate expression vectors, if needed, and stained with PKH dyes (dark green circles in Fig. 1 C.2). Cells were then replated in methylcellulose to allow the formation of second-generation MSs. The formation of MSs was monitored for up to 168 h by video microscopy. The modality of the first mitotic division was established by two criteria: the pattern of cell number progression within the forming MS (Fig. 1 C.3.1) and pattern of PKH labeling in the forming MS (Fig. 1 C.3.2).

When determining the modality of division based on cell number progression (Fig. 1 C.3.1), a 1-2-3-5 pattern of cell number progression was considered as the result of an initial asymmetric division, followed by symmetric divisions of the progenitors (see Fig. 1 D for actual images). Conversely, a 1-2-4 progression pattern was the result of an initial symmetric division. In this case, after the four-cell stage, the exact number of cells cannot be unequivocally determined in the absence of a precise 3D reconstruction. Therefore, we used 6/8 in Fig. 4 E and Fig. S2 E to indicate the number of cells originated after the four-cell stage.

When determining the modality of division based on the pattern of PKH labeling in the forming MS (Fig. 1 C.3.2), we reasoned that an asymmetric division would yield a stem-like DC that remains quiescent and therefore retains the PKH dye, whereas the progenitor-DC would divide further to yield several dull precursors. In such cases, the stem-like DC can be retrospectively identified based on intensity of PKH labeling. A schematic representation of this type of PKH staining pattern within a secondary MS is shown in panel 3.2 of Fig. 1 C.

Of note, we found that most cells from the primary MS (the progenitors) did not give rise to secondary MS, or generated only small spheroids (up to 30 cells), which were not considered in the analyses shown in the main text (depicted here as dashed, filled green circles in Fig. 1 C.3.2). Thus, only spheroids, equal or larger than 70 µM, were considered as MS and analyzed retrospectively in the time-lapse movies.

The methodology depicted in Fig. 1 C.3.1 was used in all analyses (Figs. 1 D, 4 E, 6 D, and 10, B and F; and Figs. S1 F and S2 F); in some experiments (those depicted in Figs. 1 D and 5, B, D, and E; and Fig. S1 F) the methodology depicted in Fig. 1 C.3.2 was used as an additional criterion.

Antibodies and reagents

Primary Abs for immunofluorescence (IF) were directed against: p53 (DO-1, mouse monoclonal), Sox-9 (H-90, rabbit polyclonal), CD49F (C-18, rabbit polyclonal; Santa Cruz Biotechnology); Numb (AB21, a mouse monoclonal Ab against amino acids 537–551 of hNumb [Colaluca et al., 2008] or Cell Signaling Technologies [C29G11, rabbit monoclonal]); γ-tubulin (Cy3-conjugated rabbit polyclonal, C7604; Sigma-Aldrich); phospho-histone 3 (PH3, mouse monoclonal, 14955; Abcam; rabbit polyclonal, 06–570; Millipore); CK8 (TROMA1, rat

monoclonal; produced in-house); p63 (DAK-p63, mouse monoclonal; Dako); E-cadherin (24E10, rabbit monoclonal), Slug (C19G7, rabbit monoclonal; Cell Signaling Technologies); and CK14 (AF64, rabbit polyclonal; Covance). Fluorochrome-conjugated secondary Abs were obtained from Jackson ImmunoResearch Laboratories.

Abs for immunohistochemistry (IHC) were directed against Ki-67 (SP6, rabbit monoclonal; Thermo Fisher Scientific); activated caspase-3 (Asp175, rabbit polyclonal, Cell Signaling Technologies); CK18 (C-04, mouse monoclonal; Santa Cruz Biotechnology); and CK14, Slug, Sox-9, and Numb (same as for IF).

Abs for immunoblot (IB) were directed against: vinculin (mouse monoclonal; Sigma-Aldrich), p53 (1C12, mouse monoclonal; Cell Signaling Technologies); p21 (F-5, mouse monoclonal; Santa Cruz Biotechnology); Sox-9 (AB5535, rabbit polyclonal; Millipore); GRP94 (9E10, rat monoclonal, Enzo Life Sciences); N-cadherin, β-catenin (mouse monoclonal; BD Biosciences); Fibronectin (ab299, rabbit polyclonal; Abcam); and Ki-67, Numb, Slug, and activated caspase-3 (same as for IF or IHC). In the IB experiment shown in Fig. S3 B, the panels were assembled from different lanes of the same blot by splicing out lanes loaded with additional Ctrs (indicated by a thin line). In all IB, vinculin and/or GRP94 were used as loading Ctrs.

Nutlin3 was purchased from Cayman Chemical or supplied by S. Minucci and M. Varasi (European Institute of Oncology, Milan, Italy). Cisplatin was obtained from TEVA ITALIA; the (+)-enantiomer Nutlin3b was obtained from Cayman Chemical, MG132 was obtained from Enzo Life Science, and methylcellulose (MethoCult SF M3236) was obtained from StemCell Technologies.

Treatment with Nutlin3

The concentration of Nutlin3 to be used in the in vitro experiments was established based on the data shown in Fig. 6 A and Fig. S3 B. A concentration of 10 µM Nutlin3 was sufficient to restore p53 levels and activity in the absence of any effect on cell proliferation and apoptosis, assessed by Ki-67 and activated caspase-3 levels, respectively (see Fig. 10 J for similar results obtained by IHC). A minimal effect on apoptosis, but not on proliferation, was observed at 20 µM Nutlin3, whereas 30 µM Nutlin3 caused a significant inhibition of cell proliferation and induction of apoptosis. Based on these results, a concentration of 10 µM Nutlin3 was selected to perform the described in vitro experiments. An inactive enantiomer of Nutlin3, Nutlin3b, was used as an additional control to check for potential off-target effects; Nutlin3b was inactive in all experiments at concentrations five times higher than the concentration of Nutlin3 used (Fig. S3, C and D).

For the in vivo experiments, we tailored the administration regimen (20 mg/kg injected intraperitoneally every 3 d for a total of 12 d/four treatments) to minimize the apoptotic and necrotic effects reported to be associated with higher concentrations of Nutlin3 and/or more prolonged exposure to this drug (Künkele et al., 2012). In this regard, we note that our Nutlin3 administration protocol did not affect the initial growth rate of the primary transplants (Fig. 10 H) or apoptosis (Fig. 10 J), a finding in keeping with reports demonstrating minimal, if any, antitumor effects of short-term (1–2 wk) Nutlin3 treatments (Tovar et al., 2006; Vaseva et al., 2011; Künkele et al., 2012).

Engineering of vectors and quantitative PCR

The lentiviral GFP reporter vector pTRH1-p53-dscGFP (TR502PA-1, System Biosciences), expressing an unstable GFP variant (uGFP; half-life of ∼60 min) under the control of four tandem copies of a p53-binding site upstream of a minimal CMV promoter, was used to monitor p53 activity. Cells from dissociated MSs were lentivirally transduced in suspension and allowed to form next-generation MSs for 7 d. Cells were then PKH-labeled and used for time-lapse video microscopy experiments.

The lentiviral construct harboring the Numb-DsRed fusion protein was engineered by subcloning into the pLVX puro lentiviral vector (Rubinson et al., 2003) the Numb cDNA (provided by J.M. Verdi, Maine Medical Center Research Institute, Scarborough, ME) in frame with the DsRed (from the pDsRed-Monomer-N1 vector; Clontech).

The mCMV-Numb-DsRed lentiviral construct, used in the experiments in Fig. 3 A and Fig. S1 (G and H), and expressing Numb-DsRed under the control of a CMV minimal promoter, was obtained eliminating the first 668 bases of the CMV promoter of the pLVX-puro/Numb-DsRed construct by PCR-based site-directed mutagenesis. The following oligos were used to yield the minimal CMV promoter sequence: forward, 5′-GACGCAAATGGGCGGTAGGCGTGTACGG-3′; reverse, 5′-ATCGATAAACTGGATCTCTGCTGTCCCTG-3′ (5′-GACGCAAATGGGCGGTAGGCGTGTACGGTGGGAGGTCT ATATAAGCAGAGCTGGTTTAGTGAACCGTCAGATC-3′). The construct was sequence verified.

Quantitative RT-PCR analysis was performed using the TaqMan Cells-to-CT kit (Ambion). Each sample was tested in triplicate. The ΔCt method was used to calculate the mRNA levels of each target gene normalized against two different housekeeping genes. The ΔΔCt method was used to compare the mRNA levels of each target gene, normalized to the housekeeping genes, relative to an external standard. Taqman Gene Expression Assay IDs (Applied Biosystems) were Mm00432448-m1 (p21, NM_007669), Mm00487656-m1 (mdm2, NM_010786.3), Mm02384862-g1 (nanog, NM_028016.1), Mm00468601-m1 (hes1, NM_008235), Mm00468865-m1 (hey1, NM_010423.2), Mm00469280-m1 (hey2, NM_013904.1), Mm00441533-g1 (snai1, NM_011427.2), Mm00441531-m1 (snai2, NM_011415.2), Mm00442036-m1 (twist1, NM_011658.2), Mm00486906-m1 (cdh1, NM_009864.2), Mm00483213-m1 (cdh2, NM_007664.4), Mm01333430-m1 (vimentin, NM_011701.4), Mm00448840-m1 (sox9, NM_011448.4), Mm00477927-m1 (numb, NM_001136075.2), Mm00495564-m1 (zeb1, NM_011546.2), Mm99999915-g1 (GAP DH), and Mm00437762-m1 (β2-microglobulin).

shRNA experiments

shRNA lentiviral vectors, used to abrogate Numb expression, were obtained from System Biosciences (pLKO-Numb vectors): TRCN0000105735 (sh-a in Fig. S2 A; hairpin sequence: 5′-CCGG-GCA GCCTGTTTAGAGCGTAAA-CTCGAG-TTTACGCTCTAAACAGGC TGC-TTTTTG-3′) and TRCN0000105739 (sh-b in Fig. S2 A; hairpin sequence: 5′-CCGG-CAGCAGACATTCCCTCAATAT-CTCGAG-ATA TTGAGGGAATGTCTGCTG-TTTTTG-3′). Cells from dissociated MS were lentivirally transduced in suspension and allowed to form next generation MS for 7 d under puromycin selection. In all KD experiments, Ctr populations were always transduced with a Ctr shRNA-Luciferase vector (pLKO-Luc, TRCN0000072243).

Two independent mass populations (KD1 and KD2) were derived from cells silenced with sh-b (which reproducibly induced the best levels of silencing) and used for all the experiments shown in the main text. In some cases silencing (always with the oligo sh-b) was performed in immunophenotypically purified fractions of Numb-KD MECs (Fig. 7, C–H). In these cases, we refer to the silenced cells generically as Numb-KD.

Imaging studies

Time-lapse video microscopy was performed with a Scan^R screening station (Olympus-SIS) equipped with an Olympus IX 81 inverted microscope with a Hamamatsu Orca R2 Cooled CCD camera, an Olympus MT20E illumination system and an incubation chamber (Evotec/Okolab); images were acquired at 37°C with Scan^R/Xcellence software. Cells from dissociated MS were resuspended in methylcellulose

in complete medium, plated onto glass-bottom dishes and observed through a 10× 0.4 NA air objective. Differential interference contrast, PKH-, GFP-, and DsRed-epifluorescence images were collected with autofocusing procedures and compensated for focal shift. Different focal planes were recorded to prevent loss of image contrast caused by axial cell movement. Images were captured every hour for 7 d, starting 16–18 h after plating, and reconstructed using ImageJ or Matlab software (MathWorks).

Confocal analyses were performed with a Leica TCS SP5 AOBS microscope system equipped with Leica HyD (high-quantum-efficiency hybrid detector) and PMT detectors. Images were acquired at 37°C for live cells and 22°C for fixed samples using 10× 0.4 NA and 20× 0.5 NA air objectives, or 40× 1.3 NA and 63× 1.4 NA oil-immersion objectives under the control of LAS AF Software (Leica). For the IF analyses depicted in Fig. 2 (B and C), we used formalin-fixed paraffin-embedded (FFPE) consecutive serial sections from 4-wk-old murine mammary glands. For each of the series shown, an initial section was stained with mouse anti-PH3 (14955; Abcam), rabbit anti-Numb (C29G11; Cell Signaling Technologies), and Cy3-conjugated rabbit anti-γ-tubulin (C7604; Sigma-Adrich) Abs and DAPI. After the acquisition of the images, the same section was then processed by removing the coverslip, performing a new round of antigen retrieval, followed by staining with a rat anti-CK8 Ab (TROMA1), a mouse anti-PH3 Ab, and DAPI. This procedure was repeated to perform a further round of staining of the same section with a mouse anti-PH3 and Cy3-conjugated rabbit anti–γ-tubulin Abs and DAPI. A consecutive serial section was stained with a mouse anti-p63 Ab (DAK-p63; Dako) and DAPI. Multiple focal planes were acquired for each channel to ensure that signals on different focal planes were included. Because the separated centrosomes within the same cells were often located in different focal planes, because of the thickness of the nucleus, we selected only those planes allowing visualization of centrosomes in the same focal plane. Merged images represent the projection on the plane of centrosomes of confocal optical z-section slices, showing optimal signals for Numb, γ-tubulin, and PH3, acquired in different stainings of the same section. Images were analyzed with tools available via ImageJ/Fiji software, for simultaneous processing of multiple z-stacks, and Photoshop (Adobe).

Mice and histological procedures

Numb-KO mice were generated by crossing $Numb^{lox/lox}$ mice (Zilian et al., 2001; Wilson et al., 2007) with CK5-Cre mice (Ramirez et al., 2004). Targeted deletion of the *numb* allele was confirmed by PCR genotyping, as described previously (Zilian et al., 2001; Ramirez et al., 2004). NOD/SCID-IL-2R gamma chain-null mice (The Jackson Laboratory) were used as recipient for transplantation experiments (Cicalese et al., 2009; Pece et al., 2010). Mouse colonies were maintained in a certified animal facility in accordance with national and institutional guidelines.

Mammary glands, from WT and Numb-KO female mice or from outgrowths, were processed for whole-mount analysis, as described previously (Cicalese et al., 2009). In brief, inguinal glands were excised and spread onto a clean 75 × 50-mm glass polysine microscope slide (Thermo Fisher Scientific) and fixed in a 3:1 glacial acetic acid/ethanol solution at room temperature for at least 2 h or overnight. Tissues were then hydrated through 70% ethanol for at least 30 min, rinsed in distillated water twice for 10 min, and stained in carmine alum (Sigma-Aldrich) at RT overnight. Tissues were then dehydrated through a graded ethanol series (70–95–100%) for at least 30 min and finally clarified in a 1:2 benzyl alcohol/benzyl benzoate solution. Whole mounts were photographed using a stereomicroscope (Stereo Microscope SZX16; Olympus) equipped with a digital camera (Digital Sight DS-5Mc; Nikon) and acquisition software (NIS-Elements version 2.3; Nikon). HANs and infiltrating cancers were recognized and classified according to guidelines for the pathological evaluation of genetically engineered mice (Medina, 1988; Cardiff et al., 2000).

For IHC analysis, 3-µm-thick sections of FFPE mammary whole mounts or tumors were assayed with the appropriate Abs. Slides were digitally scanned with the Aperio ScanScope XT and automatically analyzed with the Aperio ImageScope IHC nuclear algorithm (Aperio Technologies). Areas containing 30–60,000 cells were analyzed, and the percentage of positive cells was calculated. Digital images were processed with Photoshop CS3.

Statistical analyses

Time-lapse video-microscopy experiments to monitor the mode (asymmetric vs. symmetric) of division. In each experiment, we calculated the percentage of asymmetric (one SC → one SC + one P, progenitor) and symmetric (one SC → two SCs) divisions for each condition, as described above and illustrated in Fig. 1 C. For the experiments depicted in Figs. 4 E, 6 D, 10, B and F, and S2 F, results are reported as the percentage of asymmetric and symmetric divisions calculated for each group in at least three independent experiments, with the corresponding standard deviations. The entire set of data was statistically analyzed using the nonparametric Fisher's exact test. For the experiments depicted in Fig. 1 D and Fig. S1 H, data were statistically analyzed using the one-sample z-test for proportions. A p-value <0.05 was considered as significant.

Time-lapse video microscopy experiments to assess the time of division. We analyzed at least three independent experiments. Results depicted in Fig. 4 E and Fig. S2 (E and F) report, for each WT/Ctr and Numb-KO/Numb-KD group, the mean value of the time of division and the standard error calculated in the three replicates. The nonparametric Kolmogorov-Smirnov test was used to analyze the distribution of data collected in the different groups. A p-value <0.05 was considered as significant.

Time-lapse video microscopy experiments to monitor p53 activity during mitosis. For the in vivo fluorescence analysis of p53 activity during the first mitotic division (Fig. 5, D and E), the mean intensity (GFP intensity) in the DCs (1 SC + 1 P, progeny in Ctr; 2 DCs, progeny in Numb/KD) at each time point was normalized to the corresponding mean intensity of the mother cell at mitosis. Lines that best approximate the time-point data up to the second mitotic division were obtained by linear regression analysis (best-fit lines, $n = 13$). The mean best fit was calculated, and the nonparametric Kolmogorov-Smirnov test was used to compare the distribution of data relative to the progeny of Ctr cells (SC and P), assuming a statistical significance level of $P < 0.05$.

Statistical analysis of other experiments. Experiments depicted in Fig. 1 (B and D); Fig. 3 (B and C); Fig. 4 E; Fig. 5 (A–C); Fig. 6 (B and D); Fig. 7 (E and F); Fig. 10 (A, C, E–I, and K); Fig. S1 F; Fig. S2 F; and Fig. S3 (A, C, and D) were performed at least in biological triplicates, whereas experiments in Fig. 4 B; Fig. 7 (G and H); Fig. 8 (F and G); Fig. S2 B; and Fig. S4 (A and C–E) were performed at least in technical triplicates. Results are expressed as mean values, and error bars indicate standard deviations. A p-value of <0.05 was considered as significant. Experiments depicted in Fig. 7 (A and B) were analyzed using the Pearson's χ^2 test of independence. Error bars are 95% confidence intervals. A p-value of <0.05 was considered as significant. Experiments depicted in Fig. 2 (B–D) were analyzed using the Fisher's exact test. Error bars are 95% confidence intervals. A p-value <0.05 was considered significant.

For transplantation studies, the frequencies were calculated by Poisson statistics, using the "StatMod" software package for the R computing environment, as described previously (Shackleton et al., 2006) and a complementary log-log generalized linear model (two-sided 95% Wald confidence intervals or, in case of zero outgrowths, one-

sided 95% Clopper-Pearson intervals), respectively. The single-hit assumption was tested as recommended and was not rejected for any dilution series ($P > 0.05$).

Online supplemental material

Fig. S1 shows the procedure for the prospective isolation of PKH^{high} cells from the mouse mammary gland and their functional characterization in vitro and in vivo as cells with intrinsic stemness traits, as opposed to PKH^{low} or PKH^{neg} cells. Also shown is the divisional history of PKH^{high} cells and the asymmetric distribution of Numb at their mitosis. Fig. S2 shows the effects of Numb ablation, through the use of two different shRNA lentiviral vectors, on selected p53 and Notch transcriptional targets. Also shown are the effects of Numb silencing on the formation and serial propagation of MSs and on the divisional history of mammosphere-forming cells in vitro. Fig. S3 shows the expression of p53 in PKH^{high} versus PKH^{neg} cells and the characterization of Nutlin3 as a pharmacological tool to revert the dysfunction of p53 caused by loss of Numb. Fig. S4 shows that loss of Numb triggers an EMT program in the mammary gland and associates with traits of faulty mammary morphogenesis in vitro and in vivo. Fig. S5 shows the effects of Numb ablation on the intrinsic content of cells in MSs, which display mammary repopulating activity in limiting dilution transplantation experiments. Also shown is the histological appearance of the mammary outgrowths generated by the orthotopic transplantation of Numb-silenced cells. Online supplemental material is available at http://www.jcb.org/cgi/content/full/jcb.201505037/DC1. Additional data are available in the JCB DataViewer at http://dx.doi.org/10.1083/jcb.201505037.dv.

Acknowledgments

We thank M. Aguet for the Numb KO mice; J. Verdi for pEGFP-FLh-Numb; S. Minucci and M. Varasi for Nutlin3; S. Freddi, M.A. Sabatino, and B. Giulini for technical assistance; A. Cicalese and L. Lanzetti for discussions; the Veterinary Facility at Istituto Europeo di Oncologia (IEO); the Imaging Service at Fondazione Istituto FIRC di Oncologia Molecolare; the Primary/Stem Cell and the Molecular Pathology Unit of the IEO Molecular Medicine Program; and P. Romano and R. Gunby for critically editing the manuscript.

This work was supported by grants from the Associazione Italiana per la Ricerca sul Cancro (AIRC - IG 11904 to S. Pece; IG 10349 and 14404 to P.P. Di Fiore, and MCO 10.000), the Italian Ministry of University and Scientific Research, the Italian Ministry of Health to S. Pece and P.P. Di Fiore; the European Research Council (Mammastem Project), the Monzino Foundation and the CARIPLO Foundation to P.P. Di Fiore; and the G. Vollaro Foundation to S. Pece.

The authors declare no competing financial interests.

Submitted: 9 May 2015
Accepted: 15 October 2015

References

Asselin-Labat, M.L., K.D. Sutherland, H. Barker, R. Thomas, M. Shackleton, N.C. Forrest, L. Hartley, L. Robb, F.G. Grosveld, J. van der Wees, et al. 2007. Gata-3 is an essential regulator of mammary-gland morphogenesis and luminal-cell differentiation. *Nat. Cell Biol.* 9:201–209. http://dx.doi.org/10.1038/ncb1530

Bello, B.C., N. Izergina, E. Caussinus, and H. Reichert. 2008. Amplification of neural stem cell proliferation by intermediate progenitor cells in Drosophila brain development. *Neural Dev.* 3:5. http://dx.doi.org/10.1186/1749-8104-3-5

Blanpain, C., W.E. Lowry, H.A. Pasolli, and E. Fuchs. 2006. Canonical notch signaling functions as a commitment switch in the epidermal lineage. *Genes Dev.* 20:3022–3035. http://dx.doi.org/10.1101/gad.1477606

Bouras, T., B. Pal, F. Vaillant, G. Harburg, M.L. Asselin-Labat, S.R. Oakes, G.J. Lindeman, and J.E. Visvader. 2008. Notch signaling regulates mammary stem cell function and luminal cell-fate commitment. *Cell Stem Cell.* 3:429–441. http://dx.doi.org/10.1016/j.stem.2008.08.001

Bowman, S.K., V. Rolland, J. Betschinger, K.A. Kinsey, G. Emery, and J.A. Knoblich. 2008. The tumor suppressors Brat and Numb regulate transit-amplifying neuroblast lineages in Drosophila. *Dev. Cell.* 14:535–546. http://dx.doi.org/10.1016/j.devcel.2008.03.004

Cardiff, R.D., M.R. Anver, B.A. Gusterson, L. Hennighausen, R.A. Jensen, M.J. Merino, S. Rehm, J. Russo, F.A. Tavassoli, L.M. Wakefield, et al. 2000. The mammary pathology of genetically engineered mice: the consensus report and recommendations from the Annapolis meeting. *Oncogene.* 19:968–988. http://dx.doi.org/10.1038/sj.onc.1203277

Caussinus, E., and C. Gonzalez. 2005. Induction of tumor growth by altered stem-cell asymmetric division in Drosophila melanogaster. *Nat. Genet.* 37:1125–1129. http://dx.doi.org/10.1038/ng1632

Cicalese, A., G. Bonizzi, C.E. Pasi, M. Faretta, S. Ronzoni, B. Giulini, C. Brisken, S. Minucci, P.P. Di Fiore, and P.G. Pelicci. 2009. The tumor suppressor p53 regulates polarity of self-renewing divisions in mammary stem cells. *Cell.* 138:1083–1095. http://dx.doi.org/10.1016/j.cell.2009.06.048

Colaluca, I.N., D. Tosoni, P. Nuciforo, F. Senic-Matuglia, V. Galimberti, G. Viale, S. Pece, and P.P. Di Fiore. 2008. NUMB controls p53 tumour suppressor activity. *Nature.* 451:76–80. http://dx.doi.org/10.1038/nature06412

Fre, S., M. Huyghe, P. Mourikis, S. Robine, D. Louvard, and S. Artavanis-Tsakonas. 2005. Notch signals control the fate of immature progenitor cells in the intestine. *Nature.* 435:964–968. http://dx.doi.org/10.1038/nature03589

Guo, M., L.Y. Jan, and Y.N. Jan. 1996. Control of daughter cell fates during asymmetric division: interaction of Numb and Notch. *Neuron.* 17:27–41. http://dx.doi.org/10.1016/S0896-6273(00)80278-0

Guo, W., Z. Keckesova, J.L. Donaher, T. Shibue, V. Tischler, F. Reinhardt, S. Itzkovitz, A. Noske, U. Zürrer-Härdi, G. Bell, et al. 2012. Slug and Sox9 cooperatively determine the mammary stem cell state. *Cell.* 148:1015–1028. http://dx.doi.org/10.1016/j.cell.2012.02.008

Insinga, A., A. Cicalese, M. Faretta, B. Gallo, L. Albano, S. Ronzoni, L. Furia, A. Viale, and P.G. Pelicci. 2013. DNA damage in stem cells activates p21, inhibits p53, and induces symmetric self-renewing divisions. *Proc. Natl. Acad. Sci. USA.* 110:3931–3936. http://dx.doi.org/10.1073/pnas.1213394110

Jerry, D.J., M.A. Ozbun, F.S. Kittrell, D.P. Lane, D. Medina, and J.S. Butel. 1993. Mutations in p53 are frequent in the preneoplastic stage of mouse mammary tumor development. *Cancer Res.* 53:3374–3381.

Karamboulas, C., and L. Ailles. 2013. Developmental signaling pathways in cancer stem cells of solid tumors. *Biochim. Biophys. Acta.* 1830:2481–2495. http://dx.doi.org/10.1016/j.bbagen.2012.11.008

Knoblich, J.A. 2010. Asymmetric cell division: recent developments and their implications for tumour biology. *Nat. Rev. Mol. Cell Biol.* 11:849–860. http://dx.doi.org/10.1038/nrm3010

Künkele, A., K. De Preter, L. Heukamp, T. Thor, K.W. Pajtler, W. Hartmann, M. Mittelbronn, M.A. Grotzer, H.E. Deubzer, F. Speleman, et al. 2012. Pharmacological activation of the p53 pathway by nutlin-3 exerts anti-tumoral effects in medulloblastomas. *Neuro-oncol.* 14:859–869. http://dx.doi.org/10.1093/neuonc/nos115

Lechler, T., and E. Fuchs. 2005. Asymmetric cell divisions promote stratification and differentiation of mammalian skin. *Nature.* 437:275–280. http://dx.doi.org/10.1038/nature03922

Mani, S.A., W. Guo, M.J. Liao, E.N. Eaton, A. Ayyanan, A.Y. Zhou, M. Brooks, F. Reinhard, C.C. Zhang, M. Shipitsin, et al. 2008. The epithelial-mesenchymal transition generates cells with properties of stem cells. *Cell.* 133:704–715. http://dx.doi.org/10.1016/j.cell.2008.03.027

McGill, M.A., and C.J. McGlade. 2003. Mammalian numb proteins promote Notch1 receptor ubiquitination and degradation of the Notch1 intracellular domain. *J. Biol. Chem.* 278:23196–23203. http://dx.doi.org/10.1074/jbc.M302827200

Medina, D. 1988. The preneoplastic state in mouse mammary tumorigenesis. *Carcinogenesis.* 9:1113–1119. http://dx.doi.org/10.1093/carcin/9.7.1113

Morrison, S.J., and J. Kimble. 2006. Asymmetric and symmetric stem-cell divisions in development and cancer. *Nature.* 441:1068–1074. http://dx.doi.org/10.1038/nature04956

Pece, S., M. Serresi, E. Santolini, M. Capra, E. Hulleman, V. Galimberti, S. Zurrida, P. Maisonneuve, G. Viale, and P.P. Di Fiore. 2004. Loss of negative regulation by Numb over Notch is relevant to human breast carcinogenesis. *J. Cell Biol.* 167:215–221. http://dx.doi.org/10.1083/jcb.200406140

Pece, S., D. Tosoni, S. Confalonieri, G. Mazzarol, M. Vecchi, S. Ronzoni, L. Bernard, G. Viale, P.G. Pelicci, and P.P. Di Fiore. 2010. Biological and molecular heterogeneity of breast cancers correlates with their cancer stem cell content. *Cell.* 140:62–73. http://dx.doi.org/10.1016/j.cell.2009.12.007

Pece, S., S. Confalonieri, R.P. Romano, and P.P. Di Fiore. 2011. NUMB-ing down cancer by more than just a NOTCH. *Biochim. Biophys. Acta.* 1815:26–43. http://dx.doi.org/10.1016/j.bbcan.2010.10.001

Pharoah, P.D., N.E. Day, and C. Caldas. 1999. Somatic mutations in the p53 gene and prognosis in breast cancer: a meta-analysis. *Br. J. Cancer.* 80:1968–1973. http://dx.doi.org/10.1038/sj.bjc.6690628

Ramirez, A., A. Page, A. Gandarillas, J. Zanet, S. Pibre, M. Vidal, L. Tusell, A. Genesca, D.A. Whitaker, D.W. Melton, and J.L. Jorcano. 2004. A keratin K5Cre transgenic line appropriate for tissue-specific or generalized Cre-mediated recombination. *Genesis.* 39:52–57. http://dx.doi.org/10.1002/gene.20025

Raouf, A., Y. Zhao, K. To, J. Stingl, A. Delaney, M. Barbara, N. Iscove, S. Jones, S. McKinney, J. Emerman, et al. 2008. Transcriptome analysis of the normal human mammary cell commitment and differentiation process. *Cell Stem Cell.* 3:109–118. http://dx.doi.org/10.1016/j.stem.2008.05.018

Rhyu, M.S., L.Y. Jan, and Y.N. Jan. 1994. Asymmetric distribution of numb protein during division of the sensory organ precursor cell confers distinct fates to daughter cells. *Cell.* 76:477–491. http://dx.doi.org/10.1016/0092-8674(94)90112-0

Rubinson, D.A., C.P. Dillon, A.V. Kwiatkowski, C. Sievers, L. Yang, J. Kopinja, D.L. Rooney, M. Zhang, M.M. Ihrig, M.T. McManus, et al. 2003. A lentivirus-based system to functionally silence genes in primary mammalian cells, stem cells and transgenic mice by RNA interference. *Nat. Genet.* 33:401–406. http://dx.doi.org/10.1038/ng1117

Shackleton, M., F. Vaillant, K.J. Simpson, J. Stingl, G.K. Smyth, M.L. Asselin-Labat, L. Wu, G.J. Lindeman, and J.E. Visvader. 2006. Generation of a functional mammary gland from a single stem cell. *Nature.* 439:84–88. http://dx.doi.org/10.1038/nature04372

Shinin, V., B. Gayraud-Morel, D. Gomès, and S. Tajbakhsh. 2006. Asymmetric division and cosegregation of template DNA strands in adult muscle satellite cells. *Nat. Cell Biol.* 8:677–687. http://dx.doi.org/10.1038/ncb1425

Skolnick, M.H., L.A. Cannon-Albright, D.E. Goldgar, J.H. Ward, C.J. Marshall, G.B. Schumann, H. Hogle, W.P. McWhorter, E.C. Wright, T.D. Tran, et al. 1990. Inheritance of proliferative breast disease in breast cancer kindreds. *Science.* 250:1715–1720. http://dx.doi.org/10.1126/science.2270486

Spana, E.P., and C.Q. Doe. 1996. Numb antagonizes Notch signaling to specify sibling neuron cell fates. *Neuron.* 17:21–26. http://dx.doi.org/10.1016/S0896-6273(00)80277-9

Spana, E.P., C. Kopczynski, C.S. Goodman, and C.Q. Doe. 1995. Asymmetric localization of numb autonomously determines sibling neuron identity in the Drosophila CNS. *Development.* 121:3489–3494.

Stingl, J., P. Eirew, I. Ricketson, M. Shackleton, F. Vaillant, D. Choi, H.I. Li, and C.J. Eaves. 2006. Purification and unique properties of mammary epithelial stem cells. *Nature.* 439:993–997. http://dx.doi.org/10.1038/nature04496

Straight, A.F., A. Cheung, J. Limouze, I. Chen, N.J. Westwood, J.R. Sellers, and T.J. Mitchison. 2003. Dissecting temporal and spatial control of cytokinesis with a myosin II Inhibitor. *Science.* 299:1743–1747. http://dx.doi.org/10.1126/science.1081412

Tosoni, D., P.P. Di Fiore, and S. Pece. 2012. Functional purification of human and mouse mammary stem cells. *Methods Mol. Biol.* 916:59–79. http://dx.doi.org/10.1007/978-1-61779-980-8_6

Tovar, C., J. Rosinski, Z. Filipovic, B. Higgins, K. Kolinsky, H. Hilton, X. Zhao, B.T. Vu, W. Qing, K. Packman, et al. 2006. Small-molecule MDM2 antagonists reveal aberrant p53 signaling in cancer: implications for therapy. *Proc. Natl. Acad. Sci. USA.* 103:1888–1893. http://dx.doi.org/10.1073/pnas.0507493103

Uemura, T., S. Shepherd, L. Ackerman, L.Y. Jan, and Y.N. Jan. 1989. numb, a gene required in determination of cell fate during sensory organ formation in Drosophila embryos. *Cell.* 58:349–360. http://dx.doi.org/10.1016/0092-8674(89)90849-0

van de Wetering, M., E. Sancho, C. Verweij, W. de Lau, I. Oving, A. Hurlstone, K. van der Horn, E. Batlle, D. Coudreuse, A.P. Haramis, et al. 2002. The beta-catenin/TCF-4 complex imposes a crypt progenitor phenotype on colorectal cancer cells. *Cell.* 111:241–250. http://dx.doi.org/10.1016/S0092-8674(02)01014-0

Vaseva, A.V., A.R. Yallowitz, N.D. Marchenko, S. Xu, and U.M. Moll. 2011. Blockade of Hsp90 by 17AAG antagonizes MDMX and synergizes with Nutlin to induce p53-mediated apoptosis in solid tumors. *Cell Death Dis.* 2:e156. http://dx.doi.org/10.1038/cddis.2011.39

Vassilev, L.T., B.T. Vu, B. Graves, D. Carvajal, F. Podlaski, Z. Filipovic, N. Kong, U. Kammlott, C. Lukacs, C. Klein, et al. 2004. In vivo activation of the p53 pathway by small-molecule antagonists of MDM2. *Science.* 303:844–848. http://dx.doi.org/10.1126/science.1092472

Weijzen, S., P. Rizzo, M. Braid, R. Vaishnav, S.M. Jonkheer, A. Zlobin, B.A. Osborne, S. Gottipati, J.C. Aster, W.C. Hahn, et al. 2002. Activation of Notch-1 signaling maintains the neoplastic phenotype in human Ras-transformed cells. *Nat. Med.* 8:979–986. http://dx.doi.org/10.1038/nm754

Westhoff, B., I.N. Colaluca, G. D'Ario, M. Donzelli, D. Tosoni, S. Volorio, G. Pelosi, L. Spaggiari, G. Mazzarol, G. Viale, et al. 2009. Alterations of the Notch pathway in lung cancer. *Proc. Natl. Acad. Sci. USA.* 106:22293–22298. http://dx.doi.org/10.1073/pnas.0907781106

Wilson, A., D.L. Ardiet, C. Saner, N. Vilain, F. Beermann, M. Aguet, H.R. Macdonald, and O. Zilian. 2007. Normal hemopoiesis and lymphopoiesis in the combined absence of numb and numblike. *J. Immunol.* 178:6746–6751. http://dx.doi.org/10.4049/jimmunol.178.11.6746

Zhong, W., J.N. Feder, M.M. Jiang, L.Y. Jan, and Y.N. Jan. 1996. Asymmetric localization of a mammalian numb homolog during mouse cortical neurogenesis. *Neuron.* 17:43–53. http://dx.doi.org/10.1016/S0896-6273(00)80279-2

Zilian, O., C. Saner, L. Hagedorn, H.Y. Lee, E. Säuberli, U. Suter, L. Sommer, and M. Aguet. 2001. Multiple roles of mouse Numb in tuning developmental cell fates. *Curr. Biol.* 11:494–501. http://dx.doi.org/10.1016/S0960-9822(01)00149-X